International Journal of Nanomedicine

Dovepress

open access to scientific and medical research

Open Access Full Text Article

ORIGINAL RESEARCH

Carvacrol-Loaded Phytosomes for Enhanced Wound Healing: Molecular Docking, Formulation, DoE-Aided Optimization, and in vitro/in vivo Evaluation

Ahmed Mowafy Tafish[1,2], Mohamed El-Sherbiny[3,4], Ahmed A Al-Karmalawy[5,6], Osama Abd El-Azeem Soliman[1], Noha Mohamed Saleh[1]

[1]Department of Pharmaceutics, Faculty of Pharmacy, Mansoura University, Mansoura, 35516, Egypt; [2]Department of Pharmaceutical Technology, Faculty of Pharmacy, Horus University, New Damietta, 34518, Egypt; [3]Department of Basic Medical Sciences, College of Medicine, AlMaarefa University, Riyadh, Saudi Arabia; [4]Department of Anatomy, Faculty of Medicine, Mansoura University, Mansoura, 35516, Egypt; [5]Department of Pharmaceutical Chemistry, Faculty of Pharmacy, Horus University, New Damietta, 34518, Egypt; [6]Pharmaceutical Chemistry Department, Faculty of Pharmacy, Ahram Canadian University, 6th of October City, Giza, 12566, Egypt

Correspondence: Noha Mohamed Saleh, Associate Professor of Pharmaceutics, Department of Pharmaceutics, Faculty of Pharmacy, Mansoura University, Mansoura, 35516, Egypt, Tel +2 01064536677, Fax +2 050 2247496, Email nunu_ramy@mans.edu.eg

Background: Despite recent advances in wound healing products, phytochemicals have been considered promising and attractive alternatives. Carvacrol (CAR), a natural phenolic compound, has been reported to be effective in wound healing.

Purpose: This work endeavored to develop novel CAR-loaded phytosomes for the enhancement of the wound healing process.

Methods: Molecular docking was performed to compare the affinities of the different types of phospholipids to CAR. Phytosomes were prepared by three methods (thin-film hydration, cosolvency, and salting out) using Lipoid S100 and Phospholipon 90H with three levels of saturation percent (0%, 50%, and 100%), and three levels of phospholipid molar percent (66.67%, 75%, and 80%). The optimization was performed using Design Expert where particle size, polydispersity index, and zeta potential were chosen as dependent variables. The optimized formula (F1) was further investigated regarding entrapment efficiency, TEM, ^{1}H-NMR, FT-IR, DSC, X-RD, in vitro release, ex vivo permeation, and stability. Furthermore, it was incorporated into a hydrogel formulation, and an in vivo study was conducted to investigate the wound-healing properties of F1.

Results: F1 was chosen as the optimized formula prepared via the thin-film hydration method with a saturation percent and a phospholipid molar percent of zero and 66.67, respectively. TEM revealed the spherical shape of phytosomal vesicles with uniform size, while the results of ^{1}H-NMR, FT-IR, DSC, and X-RD confirmed the formation of the phytosomal complex. F1 demonstrated a higher in vitro release and a slower permeation than free CAR. The wound area of F1-treated animals showed a marked reduction associated with a high degree of collagen fiber deposition and enhanced cellular proliferation.

Conclusion: F1 can be considered as a promising remedy for the enhancement of wound healing and hence it would be hoped to undergo further investigation.

Keywords: carvacrol, phospholipids, docking, phytosome, release, topical, wound healing

Introduction

The skin is considered the largest organ in the human body with several essential functions. It protects the body from the outside environment, acts as the first line of defense against the entry of microorganisms, as well as a barrier to the loss of fluids, and assists in the regulation of body temperature.[1–3] When a disruption of the anatomical structure of the skin occurs, a complicated and multifactorial process known as wound healing occurs. It is distinguished by a series of events, including inflammation, proliferation (neo-angiogenesis, granulation, re-epithelialization), and finally, maturation with

Received: 6 June 2023
Accepted: 1 October 2023
Published: 12 October 2023

Graphical Abstract

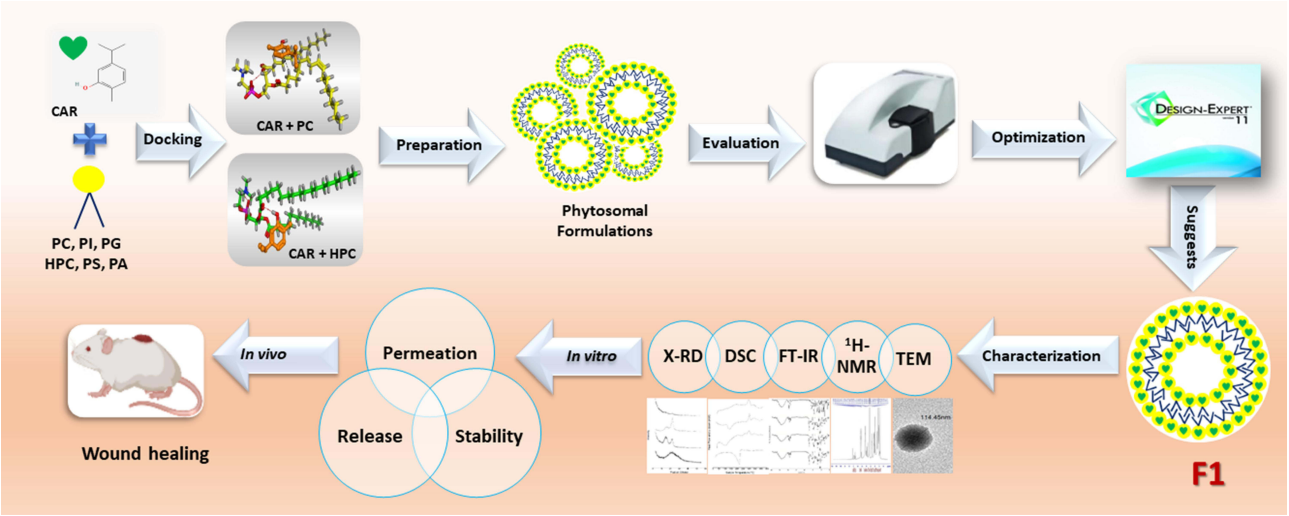

scar remodeling (cicatrization). All of these processes flow to complete wound healing and restore the skin's organized anatomical and functional status.[4]

The process of wound healing can be improved by the application of natural phytochemicals with bioactive characteristics. Various studies on the antioxidant, anti-inflammatory, antibacterial, and pro-collagen synthesis effects of phytochemicals on wound healing have been completed. Different chemical families, such as alkaloids, essential oils, flavonoids, tannins, terpenoids, saponins, and phenolic compounds have versatile bioactivity.[5] The former bioactive substances have unique roles during wound healing. For instance, phenolics, tannins, and flavonoids have antiseptic and antibacterial properties,[6] whereas saponins can improve the production of pro-collagen.[7] These phytochemicals can control one or more stages of the healing process. Additionally, the skin's outermost layers can absorb them quickly.[8] Such phytochemicals can be used over unnaturalness or manufactured chemicals due to their low cost, few side effects, patient acceptability, enhanced bioavailability, and efficacy.[9,10]

Carvacrol (CAR) is a natural monoterpene phenolic compound found in the oregano essential oil (EO). It is reported that CAR is involved in the initial stage of wound healing even though it can modulate the other two phases.[11] In the initial stages, CAR controls the release of pro-inflammatory cytokines, enhances the release of IL-10, an anti-inflammatory cytokine,[12] and inhibits the release of IL-4, IL-17, IL-1, and COX-2. In the other two phases of the wound healing process, CAR speeds up re-epithelialization, angiogenesis, and collagen deposition by raising transforming growth factor (TGF-β) and vascular endothelial growth factor (VEGF). Besides, CAR has antibacterial properties mainly against *Staphylococcus aureus* and *Staphylococcus epidermidis*, two significant bacteria that are also associated with wound infections, particularly skin infections.[13,14] Additionally, CAR's antioxidant capabilities enable it to counter reactive oxygen species (ROS), which adversely affect the wound healing process.[15]

A promising method to increase the effectiveness of phytochemicals for treating wounds is to incorporate them into nano-drug delivery systems (NDDS). Due to their small size and high surface-to-volume ratio, NDDS have distinctive properties with enhanced physical and chemical properties.[16,17] Several CAR-loaded NDDS such as nanoemulsions,[18,19] nanostructured lipid carriers,[20] solid lipid nanoparticles,[21,22] liposomes,[23,24] polylactic acid nanoparticles,[25] chitosan nanoparticles,[26,27] and albumin-based nanoparticles[28,29] were applied to improve CAR biological activities. However, the possible drawbacks of the above NDDS; for instance, the toxicity caused by high surfactant amounts (nanoemulsions) restricted drug loading (nanoparticles), low stability (liposomes), and the high cost of production necessitate the design of new CAR-loaded NDDS especially for wound healing.[30]

Nano-vesicles, such as phytosomes (or herbosomes), are considered innovative NDDS for wound healing even for the chronic diabetic ones with intrinsic cytocompatibility and the fastest wound closure rate.[31] Phytosomes are phyto-phospholipid complexes, obtained from the interaction between phospholipids and naturally occurring active phytochemicals.[32,33] From an economic point of view, phospholipids have a dual role as a phytochemical-complexing agent as well as a vesicle-forming unit during the preparation of phytosomes. Moreover, phytosomes show superior drug encapsulation, enhanced bioavailability, and better stability profile (due to chemical interaction between the polar head of the amphiphilic molecule and phytochemical) associated with improved pharmacological and pharmacokinetic features.[34] Beneficially, enhanced bioavailability due to a higher absorption rate could result in a lower dosage of active ingredients needed to exert a biological effect.[31]

Phospholipids play an important role in wound healing as they compromise the main component of the cellular membrane. Furthermore, they are compatible with many phytochemicals, so they can serve as drug carriers. Also, they can enhance the stability and hydrophilicity of hydrophobic drugs due to their emulsifying and wetting properties. The chemical structures of the various phospholipid sources vary depending on their classification, including natural phospholipids (egg phosphatidylcholine and soybean phosphatidylcholine), and synthetic phospholipids (hydrogenated phosphatidylcholine and synthetic phosphatidylcholine). A variety of phospholipids have provided alternatives for selecting appropriate phospholipids based on pharmacological actions and features to design drug delivery systems with improved therapeutic outcomes.[35]

To the best of our knowledge, no trials have been conducted to unify the merits of both CAR and phospholipids to study the heightened wound-healing activity of CAR-loaded phytosomes. Considering the above facts, the current work aimed to develop a CAR-loaded phytosomal formulation to enhance the wound-healing activity of CAR. To accomplish our aim, molecular docking was applied first to acquire the appropriate phospholipids, and then the preparation of phytosomes was completed using different variables. Furthermore, DoE-optimized phytosomal formulation was subjected to an extensive appraisal that extended to in vitro/in vivo evaluation.

Materials and Methods

Carvacrol (Product No. W224511), PCNA primary antibody (rabbit polyclonal Anti-Proliferating Cell Nuclear Antigen antibody, SAB2701819), and Bovine serum albumin (BSA) were bought from Sigma-Aldrich Co., (St. Louis, Mo., USA). LIPOID S100 (CAS No.97281–47-5) (Soybean phosphatidylcholine) and PHOSPHOLIPON 90H (CAS No.97281–48-6) (Hydrogenated soybean phosphatidylcholine) were kindly provided by Lipoid GmbH (Ludwigshafen, Germany). Spectrapor cellulose tubing, M.W.CO: 12,000 Da was acquired from Spectrum Medical Industries Inc. (Los Angeles, USA). n-hexane 95% was purchased from (Alpha Chemika, Mumbai, India). Carbopol 934, absolute ethyl alcohol, disodium hydrogen phosphate, potassium dihydrogen phosphate, and were purchased from El-Nasr Pharmaceutical Chemicals Co. (Cairo, Egypt).

The Examination of Carvacrol/Phospholipids Binding by Molecular Docking

A molecular docking study using a drug design approach[36,37] was applied to investigate the potential binding of CAR towards different types of phospholipids. This study served as a pre-formulation step before the preparation of phytosomes. Besides, it was important to compare the affinities of the different types of phospholipids to CAR.

First, CAR and six different types of phospholipids [soybean phosphatidylcholine (PC), hydrogenated soybean phosphatidylcholine (HPC), phosphatidylinositol (PI), phosphatidylserine (PS), phosphatidylglycerol (PG), and phosphatidic acid (PA)] were extracted from the PubChem website. Each compound was introduced individually into the working window, corrected for partial charges, and energy minimized.[38,39] Then, CAR was inserted into a single database to be ready for the docking process.

Second, each one of the previously prepared phospholipids was introduced individually into the working window, where a separate docking process was applied using the database of CAR in place of the ligand.[40,41] Therefore, six different docking processes were performed to compare their docking scores. Based on our findings, PC and HPC were used for the formulation of CAR-loaded phytosomes. Lipoid S100 and Phospholipon 90H were assigned as PC and HPC, respectively.

Preparation of CAR-Loaded Phytosomes

Three methods were applied for the preparation of CAR-loaded phytosomes using three levels of saturation as well as phospholipid molar percent as illustrated in Table 1. The compositions of the prepared phytosomes are listed in Table 2.

Thin Film Hydration Method

CAR and phospholipid were dissolved in 10 mL absolute ethanol and magnetically stirred overnight. Then, the obtained mixture was refluxed under a vacuum in a 500 mL round-bottom flask using a rotary evaporator (Wheaton, Chicago, Illinois, USA) at 40°C and 120 rpm to allow the formation of a thin film. After complete evaporation of ethanol, the

Table 1 The Independent Variables with Three Levels

Independent Variables	Unit	Levels		
		Low (−1)	Intermediate (0)	High (+1)
A: Saturation percent	%	0	50	100
B: Phospholipid molar percent	%	66.67	75	80
C: Method of preparation	—	Thin film hydration	Cosolvency	Salting out

Table 2 The Experimental Design, Particle Size, Polydispersity, Zeta Potential, and Entrapment Efficiency of the CAR-Loaded Phytosomes

Formula Code	Independent Variables			Dependent Variables			EE%
	A	B	C	PZ (d.nm)	PDI	ZP (mV)	
F1	−1	−1	−1	110.1 ± 20.8	0.23 ± 0.04	−15.9 ± 3.99	96.57 ± 3.36
F2	−1	0	−1	89.98 ± 1.93	0.26 ± 0.01	−14.9 ± 2.91	98.25 ± 1.57
F3	−1	1	−1	85.48 ± 2.46	0.30 ± 0.01	−10.2 ± 1.10	99.28 ± 0.98
F4	0	−1	−1	95.48 ± 12.7	0.29 ± 0.01	−4.56 ± 0.99	94.16 ± 1.73
F5	0	0	−1	89.12 ± 4.05	0.29 ± 0.03	−4.96 ± 1.67	94.99 ± 2.30
F6	0	1	−1	98.30 ± 4.62	0.29 ± 0.03	−2.24 ± 0.64	95.01 ± 2.51
F7	1	−1	−1	256.9 ± 22.0	0.41 ± 0.20	−9.92 ± 1.15	94.68 ± 0.54
F8	1	0	−1	142.5 ± 16.2	0.34 ± 0.14	−5.78 ± 0.39	96.66 ± 3.15
F9	1	1	−1	142.7 ± 7.67	0.22 ± 0.02	−2.05 ± 0.69	94.61 ± 4.81
F10	−1	−1	0	69.85 ± 2.36	0.24 ± 0.01	−10.4 ± 2.57	97.44 ± 2.57
F11	−1	0	0	86.36 ± 14.1	0.41 ± 0.04	−6.25 ± 1.89	100.0 ± 0.00
F12	−1	1	0	102.9 ± 9.40	0.41 ± 0.03	−9.05 ± 4.39	100.0 ± 0.00
F13	0	−1	0	102.3 ± 13.5	0.34 ± 0.03	−2.30 ± 0.98	99.64 ± 0.53
F14	0	0	0	110.2 ± 17.8	0.34 ± 0.05	−9.46 ± 1.62	100.0 ± 0.00
F15	0	1	0	137.7 ± 6.69	0.52 ± 0.01	−5.46 ± 1.00	100.0 ± 0.00
F16	1	−1	0	602.9 ± 48.9	0.52 ± 0.05	−2.53 ± 1.05	95.80 ± 2.84
F17	1	0	0	286.9 ± 38.7	0.47 ± 0.05	−2.67 ± 0.18	99.03 ± 1.67
F18	1	1	0	263.2 ± 13.6	0.36 ± 0.07	−7.39 ± 1.34	99.80 ± 0.33

(*Continued*)

Table 2 (Continued).

Formula Code	Independent Variables			Dependent Variables			EE%
	A	B	C	PZ (d.nm)	PDI	ZP (mV)	
F19	−1	−1	−1	186.2 ± 9.08	0.37 ± 0.08	−12.9 ± 1.72	98.47 ± 1.52
F20	−1	0	−1	141.1 ± 15.2	0.42 ± 0.04	−9.30 ± 0.95	98.69 ± 1.23
F21	−1	1	−1	132.0 ± 4.81	0.41 ± 0.05	−11.6 ± 2.49	99.82 ± 0.31
F22	0	−1	−1	115.4 ± 16.4	0.33 ± 0.03	−6.87 ± 0.14	99.10 ± 0.78
F23	0	0	−1	101.0 ± 2.60	0.35 ± 0.06	−3.73 ± 0.48	99.85 ± 0.25
F24	0	1	−1	122.8 ± 1.80	0.37 ± 0.05	−9.64 ± 0.96	100.0 ± 0.00
F25	1	−1	−1	251.5 ± 18.8	0.35 ± 0.09	−4.97 ± 0.15	97.40 ± 1.96
F26	1	0	−1	276.5 ± 23.5	0.28 ± 0.10	−2.22 ± 0.05	96.98 ± 2.42
F27	1	1	−1	169.6 ± 15.7	0.22 ± 0.02	−3.69 ± 1.80	97.02 ± 2.14

Note: Each value represents mean ± SD (n=3).
Abbreviations: A, saturation percent; B, phospholipid molar percent; C, method of preparation; PZ, particle size; PDI, polydispersity index; ZP, zeta potential; EE%, entrapment efficiency.

resulting thin film was stored in the refrigerator overnight and then hydrated with 10 mL of distilled water to obtain the phytosomal suspension. Sonication was carried out at 60% amplitude for 3 minutes with a probe sonicator (SONICS Vibra-cell, Sonic & Materials, INC, USA).[42]

Cosolvency Method

In two beakers, CAR and phospholipid were dissolved separately in 5 mL of absolute ethanol. After that, the phospholipid solution was added dropwise to CAR under magnetic stirring (Heidolph, USA). The obtained mixture was allowed to evaporate for 1h. Then, the mixture was hydrated with 10 mL of distilled water. Sonication was carried out at 60% amplitude for 3 minutes.[43]

Salting Out Method

Ethanol (5 mL) was utilized to dissolve both CAR and phospholipid with magnetic stirring. Then, n-hexane was added dropwise to precipitate and separate phytosomes. After that, the mixture was hydrated with 10 mL of distilled water. Sonication was carried out at 60% amplitude for 3 minutes.[44]

Characterization of CAR-Loaded Phytosomes

Particle Size and Polydispersity Index

Particle size (PZ) and polydispersity index (PDI) were measured employing dynamic light scattering (DLS) at a fixed angle of 90° and a temperature of 25° C using Zetasizer (ZEN 3600, Malvern Instruments Limited, UK). All samples were diluted appropriately, and the experiments were done in triplicate.

Zeta Potential

The zeta potential (ZP) of the prepared phytosomes was measured using photon correlation spectroscopy operated at 25°C by Zetasizer (ZEN 3600, Malvern Instruments Limited, UK). Samples were properly diluted, and the experiments were done in triplicate.

Entrapment Efficiency

Entrapment efficiency (EE%) of the prepared phytosomes was determined using the ultrafiltration technique.[45] Briefly, 3 mL of the phytosome formulation was transferred to an Amicon Ultra-4 Centrifugal Filter tube (10 kDa MWCO) and

then centrifuged for 60 minutes at room temperature (Sigma Laborzentrifugen GmbH, Germany). The ultrafiltrate was separated, diluted, and measured spectrophotometrically at 273 nm (UV/VIS spectrophotometer, JASCO, Tokyo, Japan). The following equation was used to compute the EE%:

$$EE\% = \frac{T - F}{T} \times 100$$

Where T is the total amount of CAR and F is free CAR detected in the ultrafiltrate (Unentrapped CAR).

Optimization of CAR-Loaded Phytosomes

Design Expert software (version 11.0.0; Stat-Ease Inc., Minneapolis, MN, USA) was used to explore the collective effect of three independent variables with three levels: Saturation percent (A) (0%, 50%, and 100%), Phospholipid molar percent (B) (66.67%, 75%, and 80%), and method of preparation (C) (thin-film hydration, cosolvency, and salting out) on three dependent variables: PZ, PDI, and ZP. Table 1 illustrates the three levels of the three independent variables expressed by the coded factor levels as −1 (low level), 0 (intermediate), and +1 (high level). Each response was conducted in triplicate (n = 3), and the data were expressed as mean ± SD. The run numbers with the applied variables and levels are illustrated in Table 2. Then, the design outcomes were confirmed by repeating the solution with the highest desirability and comparing the predicted values for dependent variables with the actual ones. The optimized formula (F1), composed of CAR and Lipoid S100 at 1:2 ratios, was further studied.

Morphological Characteristics of the Optimized Formula (F1)

Morphological features were observed using transmission electron microscopy (TEM) (JOEL 2100, Tokyo, Japan), working at an accelerating voltage of 120 kV. The sample was diluted appropriately, and then a drop was placed onto a carbon-coated copper grid to leave a thin film of the liquid sample. Then, the obtained film was stained with 1% osmium tetroxide. The excess stain was removed with filter paper to allow drying. The stained film was examined and photographed.

Solid Characterization of the Optimized Formula (F1)

Encapsulation of CAR within the prepared phytosomes was examined employing proton nuclear magnetic resonance (^{1}H-NMR), Fourier transform-infrared spectroscopy (FT-IR), differential scanning calorimetry (DSC), and X-ray diffractometry (X-RD). F1 was freeze-dried (Freeze dryer, SIM FD8-8T, SIM International, USA). Then, it was examined in comparison to samples of CAR, Lipoid S100, and CAR-Lipoid S100 physical mixture (physical mixture).

Proton Nuclear Magnetic Resonance Analysis

The carbon-hydrogen framework of individual components and F1 was compared using proton nuclear magnetic resonance (^{1}H-NMR). On a 400 MHz high-resolution spectrophotometer (Bruker Daltonics Inc., MA, USA), individual samples of pure CAR, pure Lipoid S100, physical mixture, and F1 were investigated to obtain ^{1}H-NMR spectra.

Fourier Transform-Infrared Spectroscopy

Fourier transform-infrared (FT-IR) spectroscopy study of CAR, Lipoid S100, physical mixture, and F1 was performed using Attenuated Total Reflection (ATR) technique. ATR facilitates the use of samples directly. Briefly, the sample was located just below the fixed probe of the FT-IR spectrophotometer (Madison Instruments, Middleton, Wisconsin, USA) and scanned over the 4000–500 cm^{-1} wavenumbers region.

Differential Scanning Calorimetry

The thermal behavior of CAR, Lipoid S100, physical mixture, and F1 was analyzed to verify the formation of the phytosomal complex. The thermal analysis was carried out using differential scanning colorimetry (DSC 6000; Perkin-Elmer, Waltham, MA, USA). The samples were heated from 20 to 415°C at a 10°C/min heating rate.

X-Ray Diffractometry

X-ray diffraction (X-RD) patterns of CAR, Lipoid S100, physical mixture, and F1 were obtained using an X-ray diffractometer equipped with Cu Kα (Diano Corp., Woburn, MA, USA). The tube operated at 45 kV and 9 mA at a scanning range of 3°–55° at a 2θ angle.

Physical Stability of the Optimized Formula (F1)

The stability of F1 was assessed under different storage conditions. The phytosomal suspension was freshly prepared, packed in amber glass bottles, and stored in a refrigerator (4 ± 1°C) and at room temperature (25 ± 1°C) for 6 months. The stability of F1 was measured in terms of the physical appearance, PZ, PDI, ZP, and EE% at intervals of 0, 1, 2, 3, and 6 months.

In vitro Release Study

Modified vertical Franz diffusion cells having a diffusional surface area of 7.07 cm^2 were applied. A semipermeable cellophane membrane with an MW cutoff of 12,000–14,000 was used to separate donor and receptor half-cells. The membrane was pre-equilibrated with release media. Two release media were applied: phosphate buffer pH 5.5 and pH 7.4 representing skin and physiological pH, respectively. To secure the sink condition, 10% ethanol was added to the media. CAR (5 mg) or an equivalent amount of F1 was placed in the donor compartment. The receptor compartment was filled with 60 mL of release media. The whole system was stirred at (37 ± 0.2°C) and 100 rpm throughout the experiment using a shaking incubator (Gesellschaft für Labortechnik, Burgwedel, Germany). At predetermined time intervals, samples were withdrawn from the receptor compartment and replaced with an equal volume of fresh medium. The samples were measured spectrophotometrically at 273 nm. Each experiment was replicated three times, and the average was calculated.

The following mathematical models were used to examine the release data: zero-order, first-order,[46] Hixon-Crowell model,[47] Weibull model,[48,49] Higuchi equation,[50] and Korsmeyer-Peppas equation.[51]

Zero-order kinetics: $F = K_0 t$

First-order kinetics: $\ln(1\text{-}F) = -K_1 t$

Hixon-Crowell model: $(1 - F)^{\frac{1}{3}} = 1 - K_\beta t$

Weibull model: $Log(-\ln(1 - F)) = \beta Log(t - T_i) - \text{Log}\alpha$

Higuchi model: $F = K_H t^{\frac{1}{2}}$

Korsmeyer-Peppas model: $F = K_P t^n$

Where F specifies the fraction of CAR released in time t. K_o, K_1, K_H, β, α, Ti, K_β, K_p, and n represent zero-order release constant, first-order release constant, Higuchi diffusion constant, shape parameter, scale parameter, lag time, Hixon-Crowell release constant, Korsmeyer-Peppas release rate constant, and diffusion exponent, respectively. The model with the highest correlation coefficient (r^2) is the most popular.[52]

Ex vivo Skin Permeation Study

Adult male albino rats (180–250 g) were obtained from the Animal House of the Pharmacology Department, Faculty of Pharmacy, Mansoura University. The Research Ethical Committee at the Faculty of Pharmacy, Mansoura University approved protocols regarding animal experiments (Ethical Approval Code: 2023–39) following "The Principle of Laboratory Animal Care" (NIH publication No. 85–23, revised 1985). Also, the animal-related experiments were conducted under the Animal Research: Reporting of In Vivo Experiments (ARRIVE) principles. An electric shaver was used to remove hair from the dorsal skin. During shaving, great care was taken to avoid damaging the skin's surface. Animals were sacrificed, and their skin was excised and checked for integrity with a lamp-inspecting procedure.[53] The adipose tissue layer was rubbed with a cotton swab to eliminate it. The fresh skin was kept in phosphate buffer pH 7.4 overnight in a refrigerator at 4°C to be used the next day.[54]

Modified vertical Franz diffusion cells were designed and utilized with a diffusion area of 1.13 cm^2. The skin samples were mounted on the donor half-cells with the *Stratum Corneum* (*SC*) sides positioned towards the donor compartment, while the dermal side faced the receptor one. The receptor half-cell was filled with 60 mL of phosphate buffer pH 5.5 or

pH 7.4 containing 10% ethanol. In the donor half-cell, CAR (5 mg) or an equivalent amount of F1 was placed. The entire assembly was shaken at a speed of 100 rpm and maintained at a temperature of 37 ± 0.2°C using the shaking incubator.[55] Samples were withdrawn from each receptor compartment and replaced with an equivalent volume of fresh media at scheduled time intervals. Each experiment was repeated three times. Samples were diluted appropriately and measured spectrophotometrically at 273 nm. The cumulative amount of CAR permeated (μg/cm^2) was calculated and plotted over time.

The permeability coefficient (P) was estimated at a steady state.[56] The steady-state flux (J_{ss}) expressed in μg·cm^{-2} hr^{-1} and the permeability coefficient (P) expressed in cm/hr were determined using the slope of the linear component of the cumulative amount of CAR permeated per unit surface area versus time plot according to the following equations:

$$J_{ss} = \frac{\mathrm{dQ}}{\mathrm{dt}} / \mathrm{A}$$

$$P = \frac{\mathrm{dQ}}{\mathrm{dt}} \times \frac{1}{\mathrm{AC_D}}$$

Where A is the diffusion area (1.13 cm^2), dQ/dt is the slope of the linear region of the plot of the cumulative CAR permeated versus time (μg/hr), and is C_D the donor concentration (μg/mL).

Preparation of Phytosomal Hydrogel

F1 was loaded into a hydrogel to facilitate its topical application. Carbopol 934 was used as a gelling agent at a concentration of 1% w/w.[57] It was slowly dispersed in distilled water to avoid agglomeration and to get a homogenous dispersion. Then, the mixture was stored in a dark and cool place to allow complete gelling. A pH-adjusting agent (triethanolamine) was added gradually to obtain a clear viscous gel with a suitable pH of 7.[57] After that, F1 was incorporated into the gel at an amount equivalent to 0.7% w/w CAR.[58] Finally, the total weight of the hydrogel was completed. Similarly, plain phytosomal hydrogel and CAR-loaded hydrogel were also prepared following the above-mentioned protocol with the addition of CAR (0.7% w/w) or plain phytosomes instead of F1.

Characterization of the Phytosomal Hydrogel

Physical Appearance, Clarity, Homogeneity, and pH

The prepared hydrogel was visually inspected for its appearance, clarity, distribution, and grittiness. Additionally, pH was determined by dipping a probe of pH meter (Beckman Instrument Fullerton, CA 92634, Germany) directly into the gel.

Viscosity Measurement

The viscosity was determined using a rotary viscometer (HAAKE, GmbH Germany) equipped with a sensor system of cone and plate. Briefly, a small amount of gel was placed on the lower plate and allowed to equilibrate at 37 ± 0.2°C. Then, the gel sample was subjected to a speed (N) of 64 rpm (shear rate). The value of the torque (S) was taken from the instrument and applied to the following equation:

$$\eta = \frac{G \times S}{N}$$

where η: viscosity in (mPa·s), G: instrumental factor (14,200 mPa·s/scale grad·min), S: torque (scale grad.), and N: speed (rpm). The obtained results were calculated as a mean of triplicate values.

In vivo Wound Healing Study

Adult male albino rats (180–250 g) were obtained from the Animal House of the Pharmacology Department, Faculty of Pharmacy, Mansoura University. The Research Ethical Committee at the Faculty of Pharmacy, Mansoura University approved protocols regarding animal experiments (Ethical Approval Code: 2023–39) under the principle of laboratory animal care (NIH publication No. 85–23, revised 1985). Additionally, the study was achieved following the Animal Research Reporting of In Vivo Experiments (ARRIVE) principles. Twenty animals were accommodated under standard

laboratory conditions (room temperature 25 ± 1°C, humidity 55%, 12 light/dark cycles) and fed with a standard diet and water ad libitum. The animals were equally divided into five groups (four animals per group) as follows.

- Group I: Normal animals did not receive any treatment.
- Group II: The animals were treated with plain phytosomal hydrogel.
- Group III: The animals were treated with CAR-loaded hydrogel.
- Group IV: The animals were treated with F1-loaded hydrogel.
- Group V: Positive control; the animals were treated with marketed cream (Fucidin).

For wound creation, the animals were anesthetized using intramuscular injection of Ketamine hydrochloride (0.1 mg/g body wt) and Xylazine (0.01 mg/g body wt) to undergo a surgical procedure. After shaving back hair and disinfection (70% ethanol), a full-thickness circular lesion (Ø = 2 cm) of skin, 1 cm below the bone prominence, was excised by dissecting scissors and forceps. The wound was cleaned, disinfected, and covered with sterile gauze, which was fixed with circular, adhesive bands. Twenty-four hours after the wound creation, the topical application had been started and repeated daily for 14 days.[59–61]

Macroscopic Examination and Wound Area Analysis

After wounding, the phases of wound healing were appraised morphologically from Day 0 to the 14th Day. So, the wounds were photographed by a digital camera on Days 0, 3, 5, 7.10, and 14 after wounding. The obtained photos were analyzed by an image analysis software; ImageJ 1.53t to calculate the wound surface area quantitatively. The original wound area on Day 0 was defined as A_0, and the remaining wound area on the indicated Day was defined as A_n. To express the wound healing progression, the percentage of wound closure and/or the percentage of wound remaining were calculated. The percentage of wound closure[62] and the percentage of wound remaining[63] were calculated as follows.

$$\%\ \text{wound closure} = \frac{A_0 - A_n}{A_0} \times 100$$

$$\%\ \text{wound remaining} = \frac{A_n}{A_0} \times 100$$

Histological Examination

Following the anesthetic method mentioned above, a tissue sample was taken from the healed incision on Day 14, preserved in 10% formalin, embedded in paraffin wax, and sectioned at 4.0 μm. Then, the sections underwent two washes in distilled water after being dehydrated with increasing concentrations of ethanol. The sections were stained with hematoxylin–eosin (H&E) to determine the basic phases of the healing process. Moreover, Masson's trichrome staining (MT) procedure was applied to estimate the level of collagen deposition in the re-epithelialized skin. Then, the sections were examined microscopically (Leica DMR 3000; Leica Microsystem, Hicksville, NY 11801, USA).[64,65]

Immunohistochemical Staining

PCNA primary antibody was used for the detection of basal keratinocyte proliferation. Briefly, the tissue section was blocked in 3% normal goat serum, 0.3% Triton X-100, and 0.1% BSA in phosphate buffer saline. Then, the primary antibody against PCNA, diluted to 1:100, was incubated with the section for 24 h at 4°C. The goat anti-mouse IgG (secondary antibody) for the primary antibody was then incubated for 1h at room temperature. After that, the sections were stained with hematoxylin, washed, dehydrated, treated with dimethylbenzene, and preserved for microscopic examination.[64,65]

Neo-angiogenesis was identified by measuring the mean area percent of collagen fiber deposition and the mean area percent of PCNA. Six images from six non-overlapping fields of each animal in each group were assessed using Image-Pro Plus software version 6.0 (Media Cybernetics Inc., Bethesda, Maryland, USA).

Statistical Analysis

Statistical analysis and graphical representation were completed using GraphPad Prism version 8 (Graph-Pad Software, San Diego, CA, USA). One-way analysis of variance (ANOVA) followed by the Tukey-Kramer multiple comparisons

test was applied. Data are represented as mean ± S.E. Spearman correlations were used to correlate various variables, and a p-value <0.05 was considered significant.

Results and Discussion

By the analysis of the binding scores of the six applied docking processes, it was observed that the descending order for affinities of the tested phospholipids towards the target (CAR) was as follows: PC > PI > PG > HPC > PS > PA. Their binding scores were found to be −3.51, −3.50, −3.43, −3.41, −3.33, and −3.32 kcal/mol, respectively. PC is the most frequently used phospholipid among others to prepare phospholipid complexes.[66] This is due to its amphipathic properties; besides, it is a very crucial component of cell membranes with apparent biocompatibility and low toxicity as well. It was noted that PC achieved the best binding score towards CAR (−3.51 kcal/mol). Therefore, we decided to use PC in the formulation of phytosomes. Also, HPC was selected to compare it with the superior unsaturated one (PC) and to give a broader and clearer explanation of the saturation effect as well. The binding interaction scores of CAR towards PC or HPC are manifested in Table 3.

Herein, the docking suggested the binding interactions of a single molecule of unsaturated or hydrogenated phosphatidylcholine towards a single molecule of CAR as shown in Figure 1. It was clear that the PC molecule formed a hydrogen-pi bond with the phenolic ring of CAR. However, the carbonyl group of HPC formed a hydrogen bond with the hydroxyl group of CAR. Notably, the previously described binding interactions are different from the full process of phytosome formation where these bound molecules (dimeric ones) orient themselves in specific pathways to complete the final shape of the vesicular structure of phytosomes. To sum up, molecular docking was used as a pre-formulation step to predict the affinity between CAR and different phospholipids. Such a study could save our time and effort as well as direct the design of subsequent studies.

In our study, the CAR-loaded phytosomes were successively formulated by three methods, and the three responses; PZ, PDI, and ZP were evaluated. We aimed to optimize the developed CAR-loaded phytosomes. To fulfill such demands, the responses were analyzed to offer a statistically reliable mathematical model and identify the response interactions. Table 2 documents the response variables of the CAR-loaded phytosomes. Using Design Expert software, the experimental data were statistically analyzed. Transformation is applied to the response data based on the analysis of the Box-Cox plot to ensure that all data lie within the 95% confidence interval.[67] The performed transformations include inverse ($\lambda = -1$) for PZ and inverse square root ($\lambda = -0.5$) for PDI. Following the transformation, the most desirable mathematical model was selected based on statistical goodness-of-fit. The optimal formula was found to be F1 with a saturation percent of zero and a phospholipid molar percent of 66.67 and prepared via the thin-film hydration method.

The PZ is a key parameter in determining the release profile, stability, and bioavailability of phytochemicals.[68] The mean PZ of the prepared formulations was found to be in the range of 69.85 ± 2.36 nm to 602.9 ± 48.9 nm, where smaller PZ up to 300 nm is favorable for deeper skin penetration.[69,70] The quadratic model, having a value of R^2 0.914, was found the best fit. Based on the analysis of data, an empirical second-order polynomial equation was produced, which in the form of coded factors, is as follows:

$$1/(PZ) = +0.0097 - 0.0027A + 0.0002B + 0.0011C\,[1] + 0.0001C\,[2] + 0.0006AB + 0.0003AC\,[1] - 0.0018AC\,[2] + 0.0007BC\,[1] - 0.0011BC\,[2] - 0.0023A^2 - 0.0005B^2$$

where $F = 14.53$, and $p < 0.0001$.

The analysis of data (not shown) suggested that PZ was significantly affected by saturation percent (A), method of preparation (C), interactive term of saturation percent and method of preparation (AC), and polynomial models of

Table 3 Scores of 3D Binding Interactions of CAR Towards PC and HPC

Drug	**Carvacrol**	
Phospholipid	Phosphatidylcholine (PC)	Hydrogenated Phosphatidylcholine (HPC)
Score	−3.51	−3.41

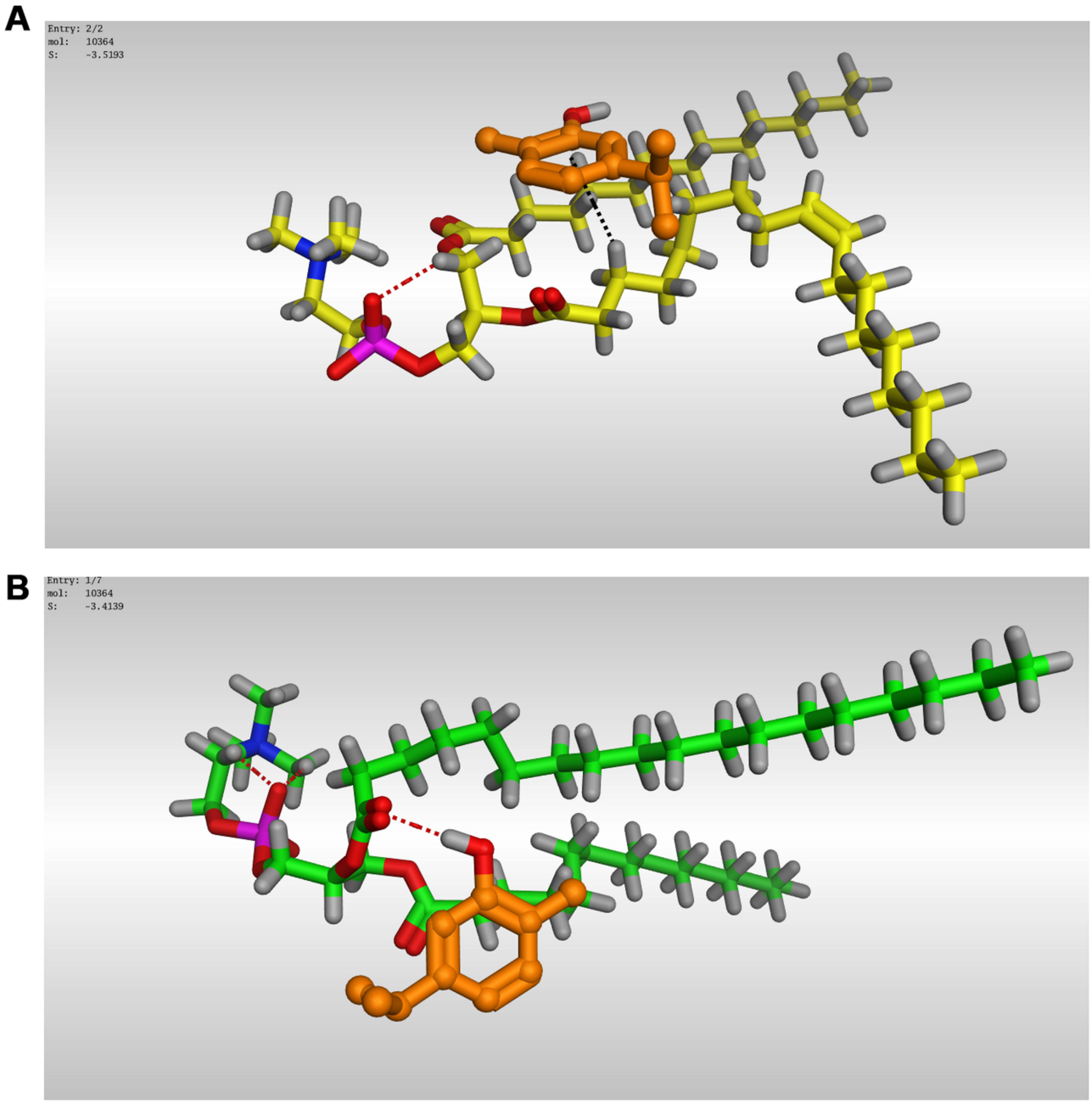

Figure 1 3D binding interactions of CAR with PC (**A**) and HPC (**B**).
Notes: The red dash represents H-bonds and the black dash represents H-pi interaction.
Abbreviations: CAR; Carvacrol, PC; Phosphatidylcholine, HPC; Hydrogenated phosphatidylcholine.

saturation percent (A^2) with *p*-values <0.05 while remaining term coefficients were not significantly affected (*p*-values >0.05). Figure 2 shows 3D and contour plots representing the effect of the interaction between the saturation percent (A) and phospholipid molar percent (B) on PZ in the case of thin film method (I), co-solvency method (II), and salting out method (III). From the equation, it can be observed that saturation percent, either linear (A) or quadratic (A^2), had a notable synergistic effect on PZ, which means that PZ increased by increasing the saturation percent of phospholipids. This finding was observed by other investigators.[71] It may be attributed to the fact that the saturated phospholipids assumed the cylinder shape, while the unsaturated phospholipids assumed the cone shape. Due to the longer inter-molecular distance, the association of these cone-shaped molecules was weaker than that of cylinder-shaped ones, which

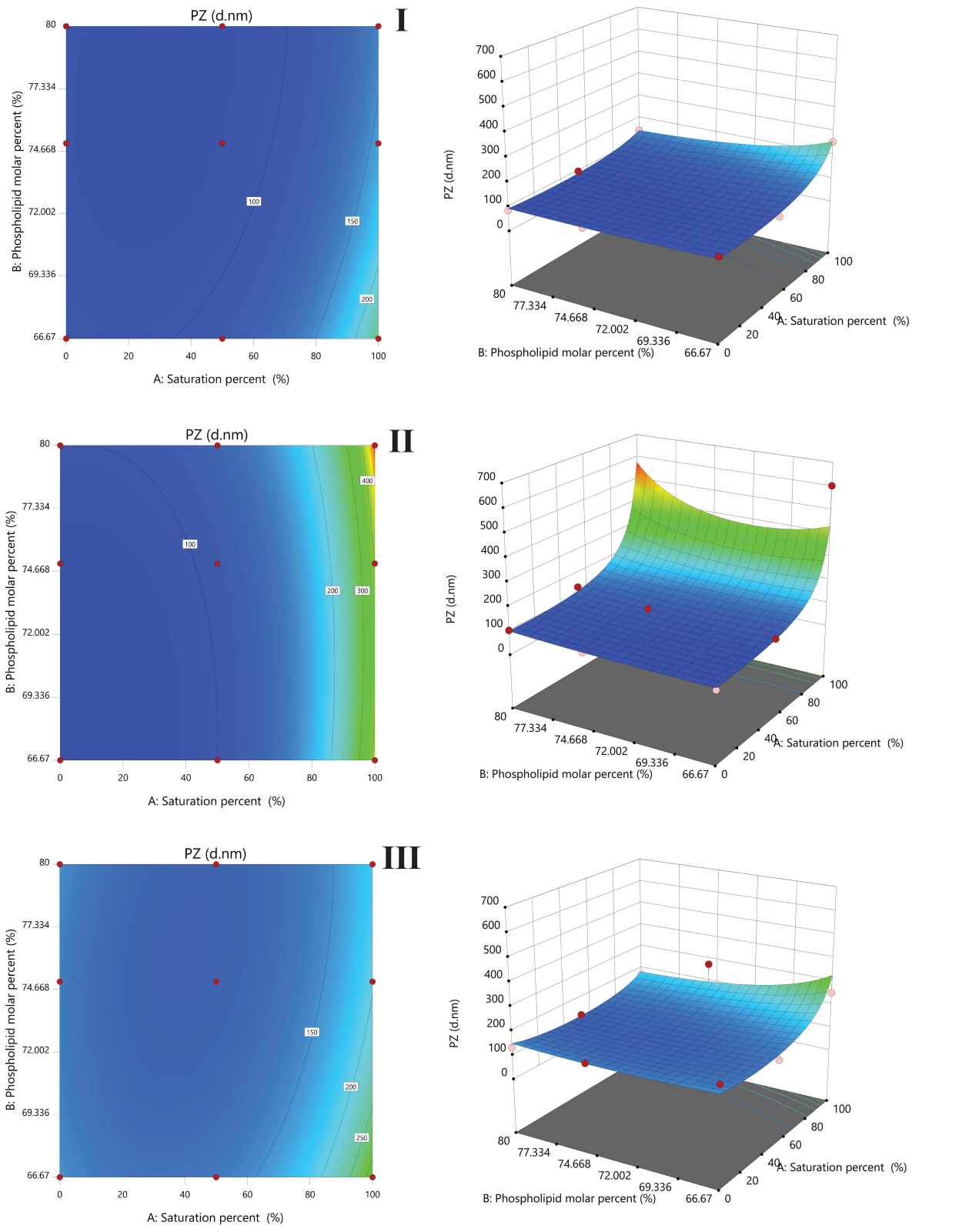

Figure 2 3D (right panel) and contour plots (left panel) represent the effect of the interaction between the saturation percent (A) and phospholipid molar percent (B) on PZ in the case of thin film method (I), co-solvency method (II), and salting out method (III).
Abbreviation: PZ, particle size.

might enhance the fluidity of the unsaturated phospholipid bilayer with reduced PZ.[72] Also, the preparation method (C) influenced PZ, where the thin-film method produced smaller PZ than other methods. The thin-film hydration method provides a larger surface area and convenient time for the phytosomal layer formation with subsequent smaller PZ without agglomeration compared to other methods. Also, the rotational movement associated with the heating of the flask had a positive impact on the thickness and homogeneity of the formed film.[73] The phospholipid molar percent (B) within the studied range from 66.67 to 80% was found to have a non-significant antagonistic effect on PZ. Probably, the increment of phospholipid molar percent (more than 80%) secures additional phospholipid molecules with their amphiphilic nature acting as surfactants for more stabilization and formation of significantly smaller vesicles.[74]

The PDI values were in the range of 0.22 ± 0.02 to 0.52 ± 0.01 (Table 2). In comparison to linear and quadratic models, a two-factor interaction model having an $R^2 = 0.861$ was found the best fit for the response (PDI). Based on data analysis, the resultant equation is given below:

$1/\sqrt{}$ (PDI) = +1.72 – 0.0192A + 0.0010B + 0.1291C [1] − 0.1169C [2] + 0.1664AB − 0.0654AC [1] − 0.0978AC [2] + 0.0494BC [1] − 0.0874BC [2]

where F = 11.74, and $p < 0.0001$.

The results suggested that PDI was significantly influenced by the linear coefficient (C) and the interactive coefficients AB and AC with *p*-values <0.001, while other variables had no prominent effect on the PDI. Figure 3 shows 3D and contour plots representing the effect of the interaction between the saturation percent (A) and phospholipid molar percent (B) on PDI in the case of thin-film method (I), co-solvency method (II), and salting out method (III). The use of response surface exploration was more valuable because it revealed how two-factor interactions affected PDI. Thus, the PDI range from 0.1 to 0.25 was obtained by decreasing both the saturation percent (A) and phospholipid molar percent (B) in thin film and cosolvency methods. On the contrary, a synchronized increase of the above variables, saturation percent and phospholipid molar percent in the case of the salting out method demonstrated a PDI range from 0.1 to 0.25. This result could be attributed to the two-factor interaction as indicated in the model equation. A PDI of 0.3 and less is thought to be appropriate in NDDS such as phytosomes, and it denotes a homogenous distribution of phospholipid vesicles.[75]

For the prepared CAR-loaded phytosomes, ZP values were found to be in the range of −15.92 ± 3.99 to −2.05 ± 0.69 mV as shown in Table 2. The linear model was determined to be the best-fitting model for ZP, and it was represented by the following equation:

$$ZP = -7.13 + 3.31A + 0.5553B - 0.7644C\ [1] + 0.9080C\ [2]$$

where F = 5.69, and $p < 0.01$.

From the above equation, it can be observed that factor A, B, and the high-order term (C2) have a positive effect on ZP ($p < 0.5$), while the low-order term (C1) shows a negative effect. Furthermore, it was observed that the effect of these individual variables on ZP was initiated by the saturation percent which had a major effect followed by a weak effect of the method of preparation, and the phospholipid molar percent. When the saturation percent decreases, more kinks are added to make the phospholipid tail less tightly packed. This allows more negatively charged hydroxide ions of water molecules to be adsorbed on the phospholipid tails, associated with higher negative values of ZP. On the other hand, the saturated phospholipid tail is free to move, which may cause one of the phospholipid tails to cluster with another one. The formation of hydration shells around phospholipid tails reduces the contact surface area of the phospholipid exposed to the external aqueous medium leading to a lower ZP. Such behavior is that of fatty acids where they tend to group to avoid water contact.[76] Figure 4 shows 3D and contour plots representing the effect of the interaction between the saturation percent (A) and phospholipid molar percent (B) on ZP in the case of thin-film method (I), co-solvency method (II), and salting out method (III). It is obvious that ZP values, in the range of −12 to −16 mV, were obtained by decreasing both the saturation percent and phospholipid molar percent. Hence, the negative charge of phytosomes could be considered as a sum of the negative charge of the phosphate group located on the surface and the hydroxide ion adsorbed on the tails. The magnitude of ZP could be considered a sign of stability, where large values prevent vesicle aggregation and allow re-dispersion.[77,78]

EE% is considered an indicator of the capacity and the ability of the developed systems to be efficiently loaded with the drug and, later on, deliver it adequately in a required dose.[79] EE% of the CAR-loaded phytosomes is listed in Table 2.

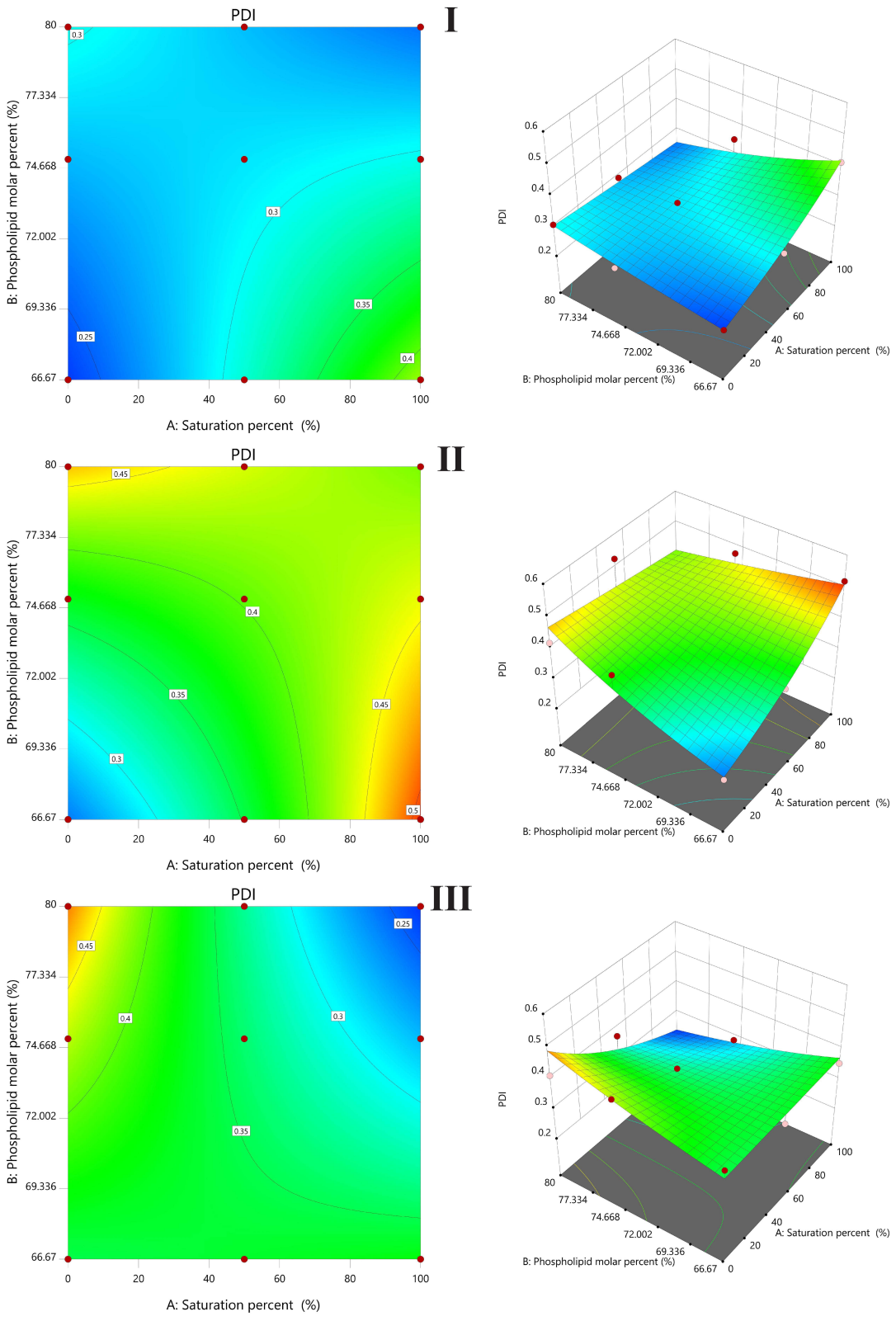

Figure 3 3D (right panel) and contour plots (left panel) represent the effect of the interaction between the saturation percent (A) and phospholipid molar percent (B) on PDI in the case of thin film method (I), co-solvency method (II), and salting out method (III).
Abbreviation: PDI, polydispersity index.

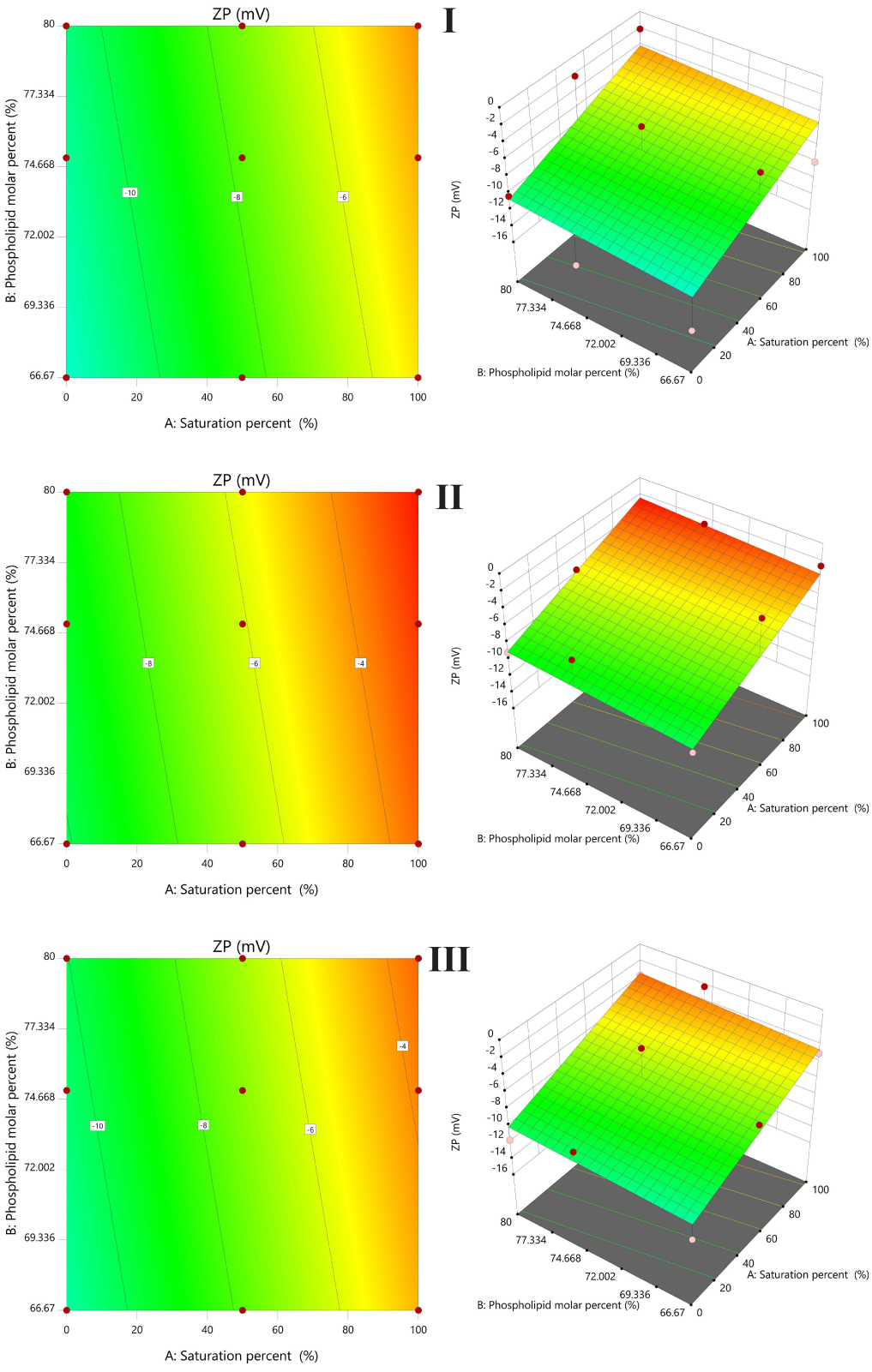

Figure 4 3D (right panel) and contour plots (left panel) represent the effect of the interaction between the saturation percent (A) and phospholipid molar percent (B) on ZP in the case of thin film method (I), co-solvency method (II), and salting out method (III).
Abbreviation: ZP, zeta potential.

It was found to range from 92.87 ± 1.21 to 100.0 ± 0.00%. For all formulations, there was no significant difference between the values of EE% ($p < 0.05$). Hence, the EE% was not considered a dependent variable during the optimization process. It can be easily understood that CAR was chemically bonded to phospholipids rather than physically entrapped, which accounts for the high values of EE%.[80] This agreed with the molecular docking results which suggested the binding interactions between PC (Lipoid S100) or HPC (Phospholipon 90H) towards CAR through a hydrogen-pi bond with the phenolic ring and a hydrogen bond with the hydroxyl group, respectively. Such a finding revealed an extra advantage of phytosomes for encapsulating a higher amount of CAR regardless of other parameters.

Each response was analyzed separately using the desirability function to construct the proper model and detect the optimal value for the evaluated parameters. The composition of the optimized formula (F1) was deduced as 66.67% phospholipid with 0% percent saturation and prepared via the thin-film hydration method. The predicted values of PZ, PDI, and ZP were 99.20 ± 12.04 nm, 0.237 ± 0.022, and −11.77 ± 3.081, respectively, with a desirability of 0.858. Thereafter, F1 was prepared by the suggested optimal values and evaluated for confirmation of the predicted model. An extremely little variation between the theoretical predictions and the measured results proved the validity of the applied model.

PZ of F1 was 120.5 ± 1.99 nm with a PDI value of 0.206 ± 0.045. An unimodal shape of size distribution curves and low value for PDI showed that the formulation was monodisperse and homogeneous. ZP of F1 was found to be −11.7 ± 1.969 mV. The observed value of ZP indicated that the preparation method and F1 components secured a suitable negative charge on the phytosome. Such charge might show repulsive forces to enhance the stability of F1.[81]

EE% of F1 was 92.87 ± 2.34%, which is consistent with the literature for other phytochemicals.[68,82] The formed bond between CAR and the polar head of Lipoid S100 indicated that the phytochemicals could be complexed with both the inner and outer membrane of the vesicular structure of F1, such a case could explain the excellent EE%.[83] As observed above, the obtained results of F1 were found to be closely related to the predicted values and in between the upper and lower prediction intervals.

The TEM microphotograph of F1 is shown in Figure 5. The formation of vesicle-like entities with spherical shapes could be proved. Additionally, a uniform size distribution without agglomeration was noticed. The PZ of F1 was found to agree with that measured by DLS. Such observation indicates that the optimized formula F1 could meet the requirements of a well-monodispersed vesicular system.

Figure 6A displays the ^{1}H-NMR spectra of CAR (I), Lipoid S100 (II), physical mixture (III), and F1 (IV) at 400 MHz. CAR ^{1}H-NMR spectrum displayed protons at δ_{ppm} 1.30 (6H, d, H-3'), 2.30 (3H, s, H-6'), 2.85 (1H, m, H-3'), 6.71 (1H, s,

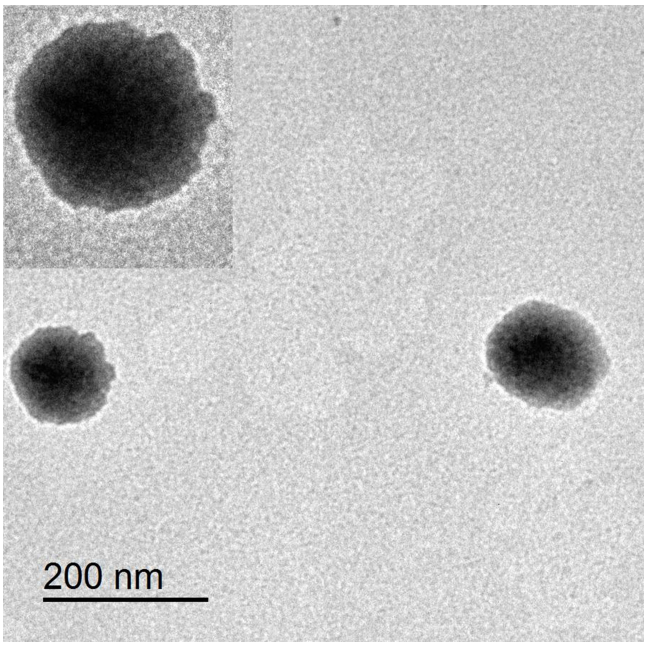

Figure 5 Microphotograph of F1.

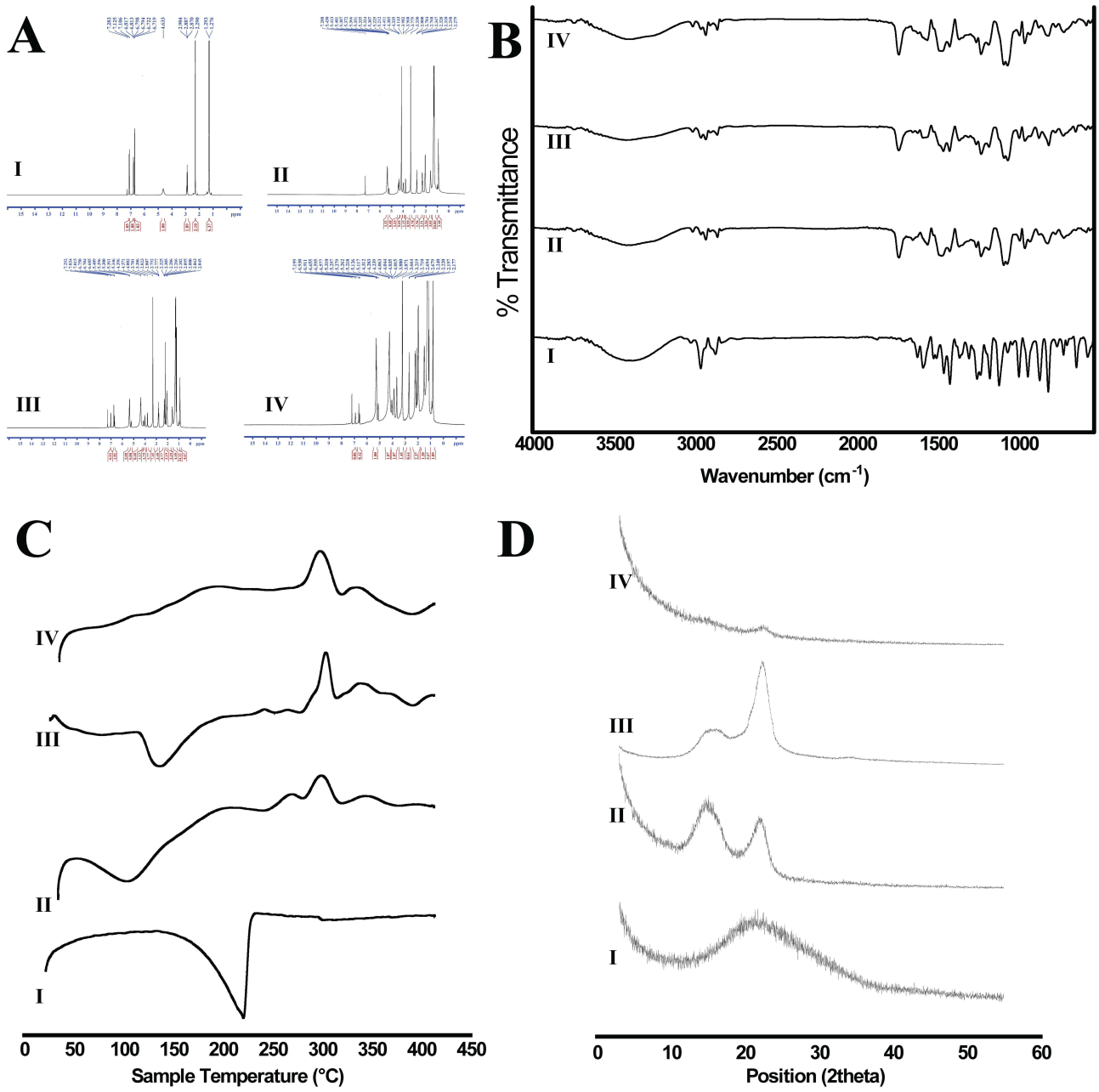

Figure 6 Solid state characterization; H[1]-NMR (**A**), FT-IR (**B**), DSC (**C**), and X-RD (**D**) of CAR (I), Lipoid S100 (II), physical mixture (III), and F1 (IV).
Abbreviations: CAR, carvacrol; F1, the optimal formula.

aromatic H-2), 6.79 (1H, dd, aromatic H-5), and 7.10 (1H, dd, aromatic H-4) (Figure 6A I).[84] On the other hand, the ^{1}H-NMR spectrum of Lipoid S100 (Figure 6A II) showed the appearance of aliphatic protons of the phospholipid and substituted amine at δ_{ppm} 0.80–3.00 (sp^3 Hs, m). The olefinic protons of the unsaturated part of the phospholipid appeared at δ_{ppm} 3.50–4.50 (sp^2 Hs, t). Also, the sp^3 protons adjacent to C=O and -–O– functional groups could be observed at δ_{ppm} 3.70–5.50.[85] However, the ^{1}H-NMR spectrum of the physical mixture (Figure 6A III) clarified the presence of the previously discussed aromatic protons of CAR in the aromatic region (δ_{ppm} 6.60–7.10) besides the identified protons of the Lipoid S100. The small observed up-field shift of the aromatic protons of CAR (δ_{ppm} 6.60 instead of 6.71) in addition to their lower intensities might be attributed to the weak physical interactions between CAR and Lipoid S100 in their physical mixture.[86]

Finally, the ^{1}H-NMR spectrum of F1 (Figure 6A IV) confirmed the formation of the phytosomal complex through the apparent decrease in the intensity of the aromatic protons of CAR, besides their further up-field shift to δ_{ppm} 6.50 instead of 6.71 due to higher shielding effects.[85] This can be explained due to the embedding of CAR molecules inside the phospholipid moieties during the formation of the phytosome complex. Briefly, this fundamentally suggests the formation of a hydrogen bond between the –OH group of CAR and the P=O group of Lipoid S100.

Figure 6B shows the FT-IR spectra of CAR (I), Lipoid S100 (II), physical mixture (III), and F1 (IV). In the FT-IR spectrum of CAR (Figure 6B I), the appearance of a broad band of –OH group (3100–3600 cm^{-1}), characteristic aliphatic sp^3 hydrogens of $–CH_3$ groups (both asymmetrical and symmetrical types), and -CH group at 2950 cm^{-1} could be observed. Also, the characteristic aromatic sp^2 hydrogens of the benzene ring at 3050 cm^{-1}, two characteristic peaks of C=C of the benzene ring at 1405 and 1430 cm^{-1}, respectively, and CO stretching at 1250 cm^{-1} could be recognized.[58,87] However, the FT-IR spectra of Lipoid S100, physical mixture, and F1 (Figure 6B II, III, and IV, respectively) exhibited the characteristic large phosphate band (P=O) at 1200 cm^{-1}, a characteristic P–O–C stretching band at 1050 and 1070, a characteristic C=O peak (in the fatty acid ester) at 1720 cm^{-1}, and $N(CH_3)_3^+$ stretching band at 950 cm^{-1}. Also, the sp^3 and sp^2 hydrogen peaks of the long fatty acid chain became more intense and blunted in shape at 2900 and 3100 cm^{-1}, respectively.[88,89]

By looking at the FT-IR spectrum of Lipoid S100, there was no clear difference between it and the physical mixture. Herein, the characteristic –OH broad band of CAR in the physical mixture disappeared in the region of the blunted sp^2 hydrogen peaks of the long fatty acid chain. This was attributed to the presence of the two items without apparent interactions, and only a slight additive effect was observed which may be attributed to the weak physical interactions.[90] On the other hand, observing the FT-IR spectrum of F1 confirmed the formation of the CAR-Lipoid S100 phytosomal complex by the remarkable broadening of the –OH band of CAR (3050–3650 cm^{-1}) which became more intense.[90] A clarified shift of –OH peak to a lower wave number (3050 cm^{-1}) in the F1 spectrum indicated the formation of a hydrogen bond between the OH group of CAR and Lipoid S100.

Figure 6C shows the DSC thermograms of CAR (I), Lipoid S100 (II), physical mixture (III), and F1 (IV). The thermogram of CAR illustrated a broad, sharp endothermic peak at 221°C, which corresponds to its boiling point.[91] While Lipoid S100 exhibits two distinct endothermic peaks; the first (105.14°C) was flat and wide, which might be due to the hot movement of phospholipids' polar head group, while the later (244.268°C) was a mild one representing the phase transition from gel to liquid crystalline state.[79,92] In the physical mixture thermogram, the endothermal peaks of both Lipoid S100 and CAR were less intense (still detectable) but shifted towards lower temperatures (65°C, 228.9°C, and 138.2°C, respectively). When the temperature of the physical mixture increased, phospholipid melted, and CAR could dissolve in it to partially form a CAR-phospholipid complex. This phenomenon is based on the theory of complex preparation by the melt-out method.[93] On the other hand, the DSC thermogram of F1 showed that the original endothermic peaks of CAR and Lipoid S100 disappeared. This finding suggested that CAR had lost its crystalline form and was molecularly dispersed on the surface and within the matrix of the phytosomes due to its interaction with Lipoid S100 through van der Waals forces and/or hydrogen bonding, singly or in combination.[94,95]

XRD is one of the most common methods used to determine the crystallinity of substances. Figure 6D shows the XRD pattern of CAR (I), Lipoid S100 (II), physical mixture (III), and F1 (IV). The CAR diffraction pattern showed sharp crystalline peaks, which are characteristic of crystalline compounds. Meanwhile, the Lipoid S100 diffractogram exhibited large two diffraction peaks, indicating an amorphous state. The physical mixture displayed some crystalline peaks and a single wide peak representing CAR and Lipoid S100, respectively. Compared to the above, the crystalline peaks disappeared in the F1. This was most likely the result of noncovalent interactions like hydrogen bonds between CAR and Lipoid S100. Such observation proved that the CAR molecules had complexed with the polar head of phospholipid molecules, and hence its crystalline characteristic was inhibited.[96]

Table 4 documents the PZ, PDI, ZP, and EE% of F1 during storage for 6 months at room temperature (25 ± 1°C), and in the refrigerator (4 ± 1°C). At zero time, PZ was 120.5 ± 1.99 nm, which significantly increased at room temperature to reach 865.5 ± 67.2 nm by the end of the experiment ($P < 0.05$). Generally, the initial ZP was −11.70 ± 1.96 mV at zero time. ZP significantly increased until it exceeded −40 mV at room temperature. This could be attributed to the dissociation of the vesicular structure of phytosomes with the liberation of free negatively charged Lipoid S100 molecules.[97,98] No significant changes in PDI were observed upon storage at room temperature. However, EE

Table 4 Stability Study of F1 Stored at Room (25 ± 1°C) and Refrigerated (4 ± 1°C) Temperatures

Temperature	Storage Time	PZ (d.nm)	PDI	ZP (mV)	EE%
Room temperature (25 ± 1°C)	Zero time	120.0 ± 1.99	0.206 ± 0.04	−11.70 ± 1.96	92.87 ± 1.21
	1st month	221.2 ± 6.58	0.265 ± 0.06	−19.93 ± 0.92	92.59 ±1.45
	2nd month	221.7 ± 1.51	0.216 ± 0.01	−17.63 ± 0.40	88.91 ± 2.53
	3rd month	157.2 ± 37.2	0.332 ± 0.17	−19.56 ± 0.50	88.54 ± 2.66
	6th month	865.5 ± 67.2	0.369 ± 0.04	−42.16 ± 1.35	86.53 ± 1.92
Refrigerator temperature (4 ± 1°C)	Zero time	120.5 ± 1.99	0.206 ± 0.04	−11.70 ± 1.96	92.87 ± 1.21
	1st month	139.2 ± 0.98	0.340 ± 0.02	−11.83 ± 0.63	94.04 ± 0.63
	2nd month	133.2 ± 1.28	0.258 ± 0.01	−16.60 ± 1.70	94.21 ± 0.57
	3rd month	122.2 ± 4.85	0.403 ± 0.03	−13.40 ± 0.52	90.57 ± 2.48
	6th month	150.8 ± 4.17	0.256 ± 0.00	−16.3 ± 1.15	90.26 ± 1.97

Abbreviations: PZ, particle size; PDI, polydispersity index; ZP, zeta potential; EE%, entrapment efficiency.

insignificantly decreased from about 93% to 86% during the storage period suggesting a reduction of the system stability and CAR leakage. This observation was consistent with that of ZP. Both indicate that the F1 stability was negatively affected by storage at room temperature.[79]

On the contrary, the PZ of F1 did not exceed 151 nm when it was stored in the refrigerator for 6 months. The ZP was insignificantly affected to become about −16 mV. The mean values of PDI remained small (<0.5) indicating homogenous size distribution.[43] This may indicate the aggregation hindrance and the physical stability of F1 during the storage period at this temperature. The stability at the refrigerator temperature was also reflected by the EE% that kept high values (≥90%). These findings might suggest that the optimized formula F1 was more stable at refrigerator temperature, preserving its effectiveness over a lengthy period of storage.

Figure 7A and B display the in vitro release profiles of CAR and F1 at two different pH settings (pH 5.5 and 7.4, respectively). Since the skin surface is known to have a pH of 5.5 (weakly acidic), this pH level may be useful in understanding how release behaves on the skin's surface. Also, the release pattern was studied at pH 7.4 to recognize the behavior in physiological circumstances. By referring to Figure 7A, it can be observed that CAR exhibited relatively a rapid release rate at pH 7.4 to reach 68% within 4 h. At pH 5.5, CAR showed a slower release rate with a percent release of 45% within 8 h. As CAR is a phenolic compound (weakly acidic) with pKa of 10.56, it might exhibit relatively higher ionization at pH 7.4 than that at pH 5.5. Hence, it was revealed that increasing pH will favor the formation of its ionizable form and thus enhance CAR release.[99]

The release profiles of CAR and the F1 were found to be similar during the first 4 h and 8 h at pH 5.5 and 7.4, respectively (Figure 7A and B). After these time points, CAR dissolution appeared to reach a plateau. On the contrary, the release of CAR from F1 at both pH values continued to reach approximately 90% within 24 h. This can be attributed to the enhanced solubility and wettability of CAR by its incorporation in the phytosomal formula (F1).[100] Accordingly, CAR aqueous solubility, which is low, was improved by the amphiphilic properties of Lipoid S100. Moreover, it was assumed that CAR transformed from its crystalline state to a partially amorphous state in the phytosomal complex (DSC finding), which might extend the release of CAR to 24 h. Furthermore, it is possible to infer that a two-step diffusion mechanism resulted in the sustained release of CAR from the phytosomal complex. First, CAR molecules dissociated from the phytosomal complex in the presence of aqueous media. Second, the dissociated free CAR molecules diffused out of the phospholipid matrix.[101] Thus, the phytosomal complex was found to significantly enhance both the rate and the extent of CAR release compared to pure CAR.[102]

Table 5 shows the release kinetics of both CAR and F1 at pH 5.5 and 7.4. It was found that CAR and F1 followed the Weibull model as indicated by the highest r^2. In the Weibull model, α is a measure of drug delivery rate, while β shows

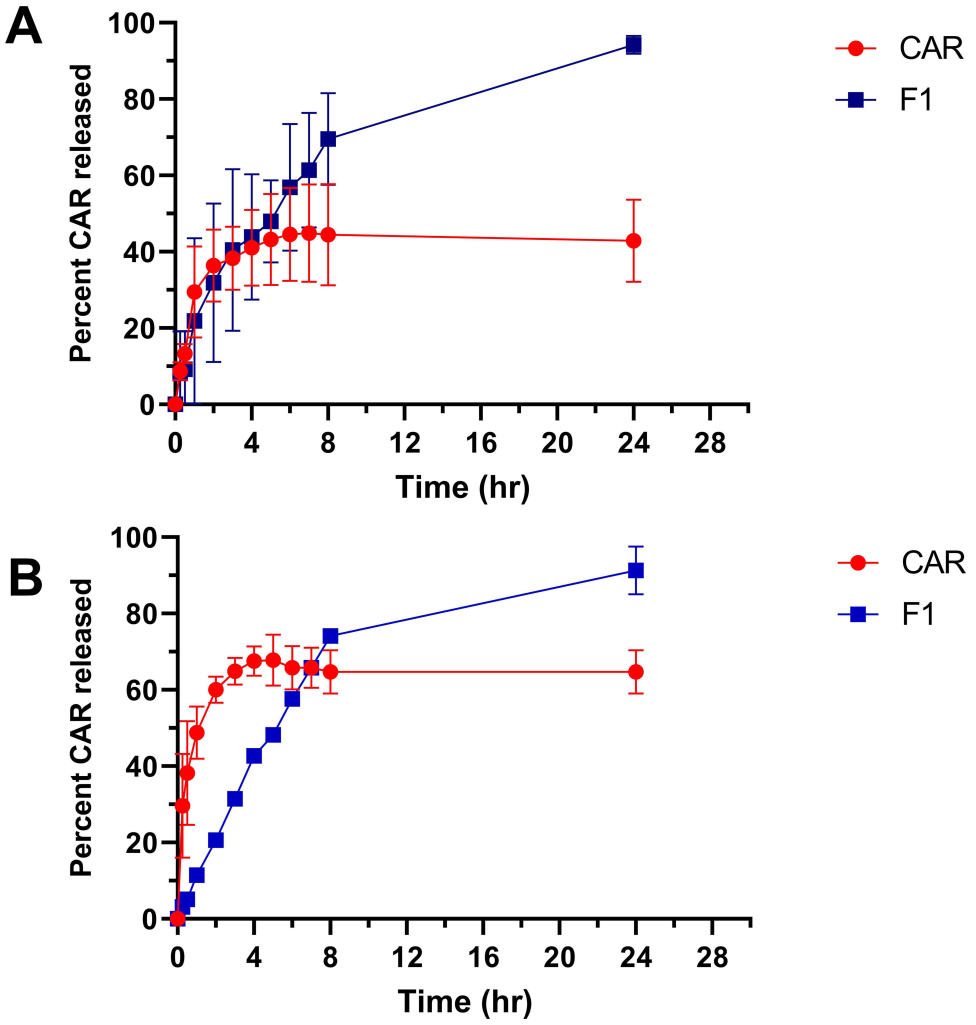

Figure 7 Release profiles of CAR and F1 in phosphate buffer pH 5.5 (**A**) and 7.4 (**B**) across cellophane membrane.
Abbreviations: CAR, carvacrol; F1, the optimal formula.

the mechanism of drug transport.[103,104] Values of the β parameter higher than 0.75 reflect a non-Fickian transport, while values of b below 0.75 suggest a Fickian diffusion of biomolecules.[105] The obtained β values indicated that the release of CAR followed a diffusion mechanism, while that of F1 occurred via a complex mechanism.[103] To further clarify the mechanism of release, the Korsmeyer-Peppas model was applied.[106]

In the Korsmeyer-Peppas model, the coefficient n indicates the type of release mechanism, and the constant k_P is dependent on the carrier properties. When $n \leq 0.45$, the Fickian diffusion mechanism dominates. In the case of $0.45 < n < 0.89$, release tracks anomalous diffusion (non-Fickian diffusion). When $n > 0.89$, a super case II transport mechanism will predominate.[107] The coefficient n of CAR was less than 0.45 and indicated a Fickian diffusion mechanism. While the coefficient n of F1 was higher than 0.89 suggesting a super case II transport mechanism. This is a relaxational release mechanism compatible with the complex release mechanism suggested by the above Weibull model.

Moreover, the correlation coefficient r^2 in the Weibull model was found to be closer to that of the Higuchi model in the case of CAR, while it was closer to that of the first-order kinetics in the case of F1, supporting the findings of the previously discussed models. Finally, comparing the release mechanisms of CAR and F1 revealed a noticeable difference. The release from the first followed Fickian diffusion, however, the second obeyed a complex mechanism. Furthermore, it was verified that the phytosome complexation technique between CAR and phospholipid altered the release of CAR not only in terms of release time or rate but also in terms of release kinetics and mechanism, supporting the findings of the in vitro release study.

Table 5 Release Kinetics of CAR and F1 at pH 5.5 and 7.4

Model \ Release Media		CAR		F1	
		pH 5.5	pH 7.4	pH 5.5	pH 7.4
ZERO	r^2	0.822	0.724	0.751	0.721
	K_0	5.751	11.07	3.655	3.947
FIRST	r^2	0.883	0.859	**0.976**	**0.958**
	K_1	−0.087	−0.214	−0.106	−0.111
H-C	r^2	0.864	0.817	0.920	0.888
	K_B	−0.025	−0.056	−0.023	−0.024
WEIBULL	r^2	**0.944**	**0.992**	**0.984**	**0.989**
	β	0.584	0.451	0.999	1.037
	α	4.224	1.586	7.212	8.059
HIGUCHI	r^2	**0.943**	**0.920**	0.962	0.924
	K_H	18.68	29.81	20.69	22.35
Release mechanism		Fickian diffusion		Non-Fickian diffusion (complex release mechanism)	
K-P	r^2	0.849	0.980	0.960	0.997
	K_P	19.92	45.78	11.70	10.88
	n	0.443	0.359	0.925	0.945
Drug transport		Fickian diffusion		Super case II transport (relaxational release mechanism)	

Note: The bold-underlined values are r^2 of the two mechanisms contributing in the release kinetics.
Abbreviations: CAR, carvacrol; F1, the optimal formula; H-C, Hixon-Crowell model; K-P, Korsmeyer-Peppas model; r^2, correlation coefficient; K_o, zero-order release constant; K_1, first-order release constant; K_β, Hixon-Crowell release constant; β, shape parameter; α, scale parameter; K_H, Higuchi diffusion constant; K_P, Korsmeyer-Peppas release rate constant; n, diffusion exponent.

Figure 8A and B show the cumulative permeated amounts (μg/cm^2) of CAR and F1 through rat skin at pH 5.5 and 7.4, respectively. The cumulative permeated amount of CAR after 24 h reached 3101.04 ± 152.9 and 4132.44 ± 379.3 μg/cm^2 at pH 5.5 and 7.4, respectively. It was found that the J_{ss} of CAR was 4.1 ± 0.45 and 8.6 ± 2.1 μg/cm^2.hr at pH 5.5 and 7.4, respectively. The cumulative amount permeated of CAR from F1 after 24 h reached 1927.79 ± 17.13 and 3221.41 ± 249.71 μg/cm^2 at pH 5.5 and 7.4, respectively. While the J_{ss} of F1 was 3.03 ± 0.53 and 7.2 ± 2.03 μg/cm^2.hr at pH 5.5 and 7.4, respectively. The J_{ss} of CAR was found to be higher than that of F1 by 1.35 folds at pH 5.5 and 1.19 folds at pH 7.4, respectively. Also, the J_{ss} of CAR at pH 7.4 was 2.07 folds higher than that at pH 5.5. It was found that the P of CAR was 4.3 ± 0.48 and 9 ± 2.2 cm/hr × 10^{-3} at pH 5.5 and 7.4, respectively, while P of F1 was 3.19 ± 0.56 and 7.59 ± 2.14 cm/hr × 10^{-3} at pH 5.5 and 7.4, respectively. At the end of permeation experiments, it was observed that *SC* remained intact (no obvious damage was noticed).

It could be concluded that the cumulative amount of CAR permeated, J_{ss} and P were higher than the corresponding ones of F1 at both pH values. This finding indicated that the permeation of CAR in the phytosomal form occurred at a slower rate than free CAR. This may be due to the time required for the following steps to occur. First, the fusigenicity and interaction between the phytosomes and *SC* were stated to be prerequisites for skin penetration.[108] Since phospholipids have a high affinity for the biological membranes, they can fuse within *SC* to disrupt its integrity and subsequently enhance skin permeation.[109] Also, CAR acts as a penetration enhancer so that it can disrupt the *SC* lipids and distribute

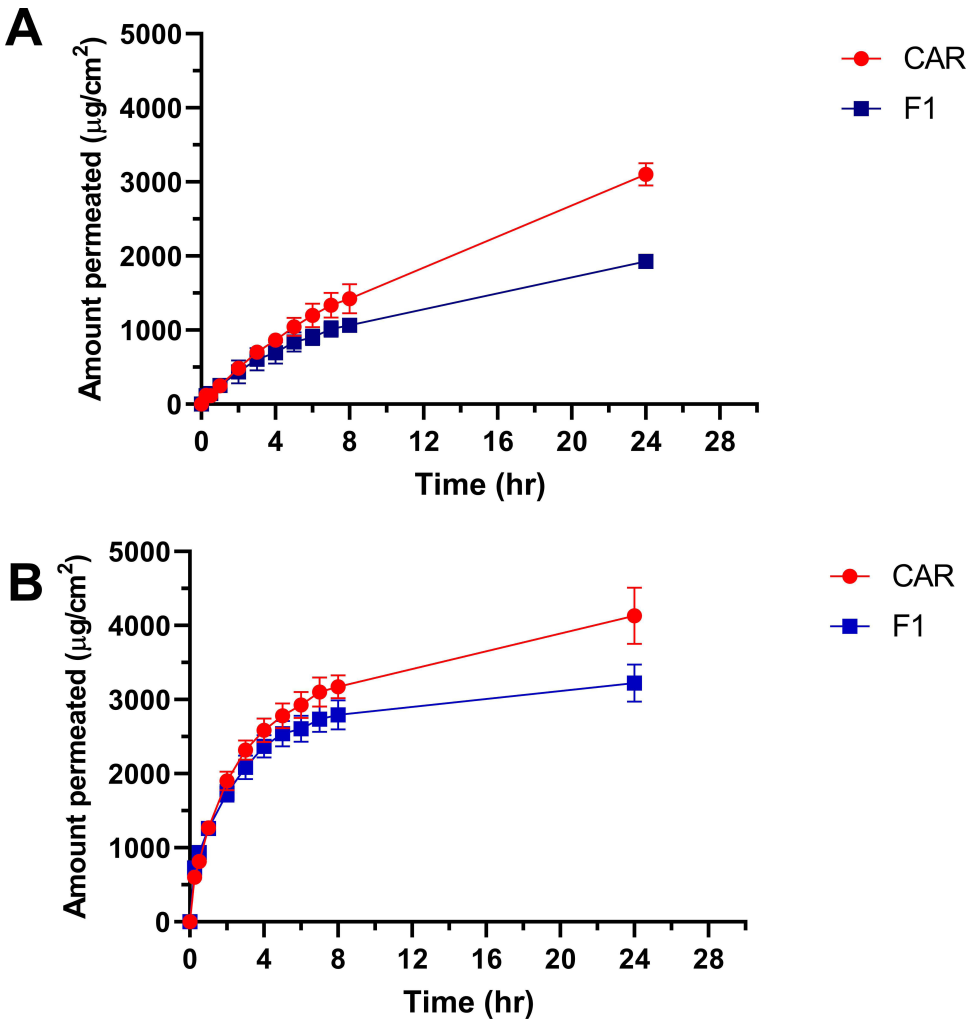

Figure 8 Cumulative amount permeated from CAR and F1 in phosphate buffer pH 5.5 (**A**) and 7.4 (**B**) across rat skin.
Abbreviations: CAR, carvacrol; F1, the optimal formula.

itself within them.[110] For F1, the penetration enhancement effect of CAR might be retarded due to its incorporation in the phytosomal complex. Second, the gradual dissociation of the phytosomal complex and release of CAR required a longer time since the skin might act as a reservoir for the phytosomal complex.[95] The J_{ss} of free CAR at pH 7.4 was found to be higher than that at pH 5.5 as increasing the pH might enhance the ionization of CAR in the receptor medium as previously described. Such a state might act as a driving force for the permeation of more CAR.

The successful development of the CAR-loaded phytosome necessitates designing a suitable dosage form for an appropriate topical application. Due to its inert nature, outstanding bioadhesive characteristics, ability to formulate high-quality pharmaceutical hydrogels and exceptional storage stability, Carbopol 934 was chosen for this purpose.[111] The consistency of the prepared hydrogel was found to be homogenous. Although all hydrogels were cloudy, the phytosomal hydrogel was cloudier than the plain phytosomal hydrogel and the CAR-loaded hydrogel. The plain phytosomal hydrogel, CAR-loaded hydrogel, and phytosomal hydrogel had pH values of 7.02 ± 0.13, 6.73 ± 0.17, and 6.54 ± 0.28, respectively. These values were relatively close to neutral pH, making it unlikely to cause skin irritation. The viscosities of the phytosomal hydrogel, the plain phytosomal hydrogel, and CAR-loaded hydrogel were found to be 3335.5 ± 33.9 mPa·S, 2647.7 ± 12.8 mPa·S, and 2240.9 ± 22.2 mPa·S, respectively. As a result, all prepared hydrogels had appropriate viscosity ranges making them suitable for topical application.[112]

Only limited trials examine the wound-healing activity of CAR in the literature. Tenci et al incorporated CAR in polymeric clay films to form a viscoelastic gel upon application.[113] Another study developed CAR-loaded

poly(caprolactone) nanoparticles, which were further incorporated in either hydrogel or dissolving microneedles.[58,114] Our study was characterized by combining CAR with phospholipid (PC; typical component of the eukaryotic cell) in an optimized manner to develop a phytosomal formulation F1 for enhancing wound healing activity.

The macroscopic appearance of the wounds throughout the experiment is shown in Figure 9. Neither an abscess nor hypertrophic scars were seen in the early phase (3rd day), middle phase (7th day), and final phase (14th day). The ability to estimate the progression of the wound area in each group during the experiment time course was made possible by the digital photographs of the wounds. The wound area was markedly reduced in the treated groups compared to the normal control group (Group I). The wounds of Group I were ulcerated throughout the dressing and left a yellowish-red surface. The best-healed groups were those who received F1-loaded hydrogel (Group IV) and marketed cream (Fucidin) (Group V). These groups quickly filled the wound's edge with healthy reddish granulation tissue, which was followed by gradual epithelialization and almost full healing by the 14th day. Group III was thought to be the second-best healing group, while Group II showed a lower degree of healing but still better than the normal control group (Group I). The normal control group had cardinal signs of inflammation that appeared at time intervals during the treatment. Principal signs of inflammation were redness, painful touching, and swelling of the skin around the borders of the wound. The least principal signs of inflammation were exhibited by Group IV, which vanished at the end of the experiment.

The wound healing progression was expressed as percentage wound closure (% wound closure) and percentage wound remaining (% wound remaining) via wound analysis as shown in Figure 10A-C respectively. The mean % wound closure at days 3, 5, 7, 10, and 14 post-wound induction was 38.01 ± 4.60, 70.70 ± 1.71, 83.42 ± 0.15, 93.79 ± 0.86, and

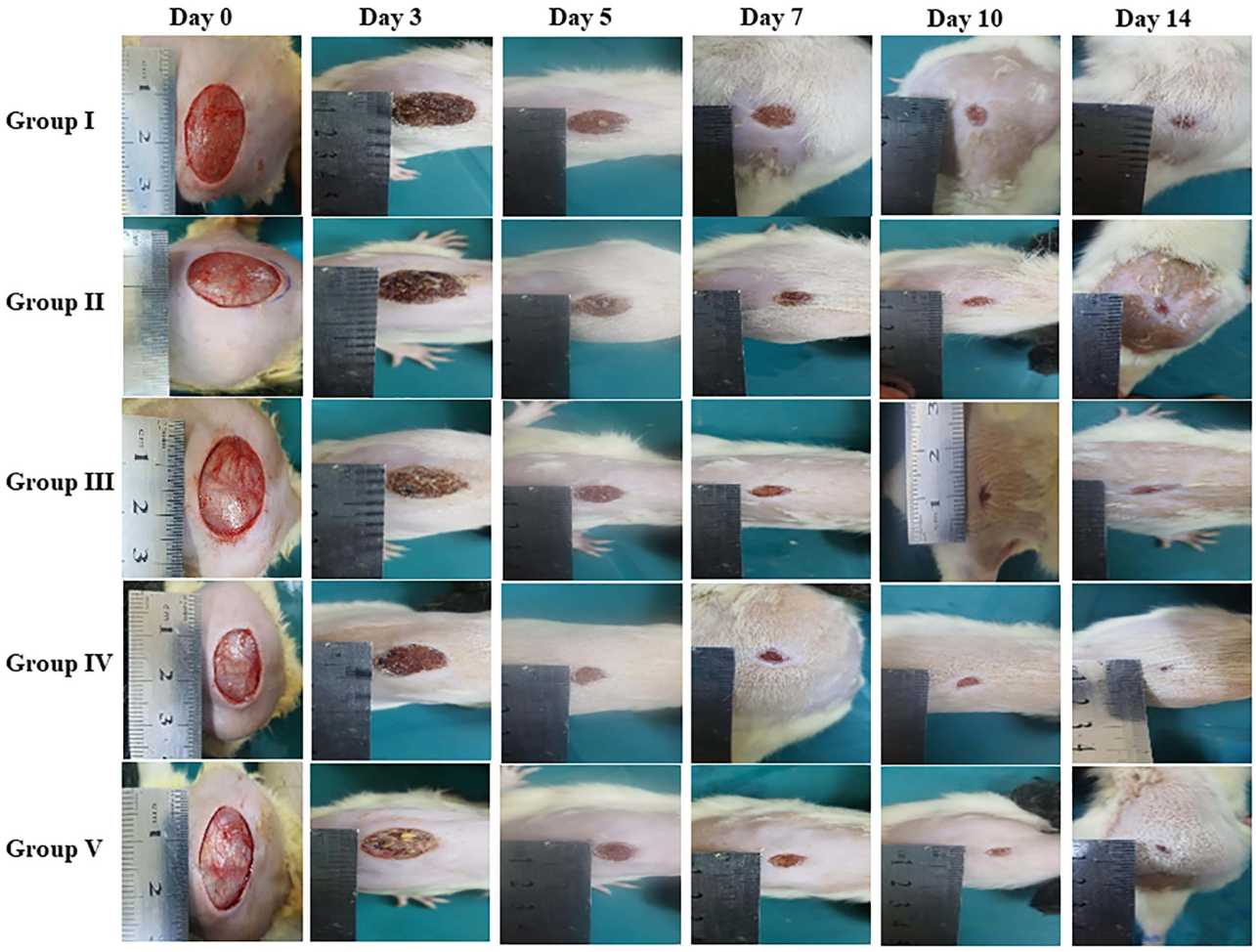

Figure 9 Macroscopic evaluation of wounds throughout 14 days of Groups I–V.

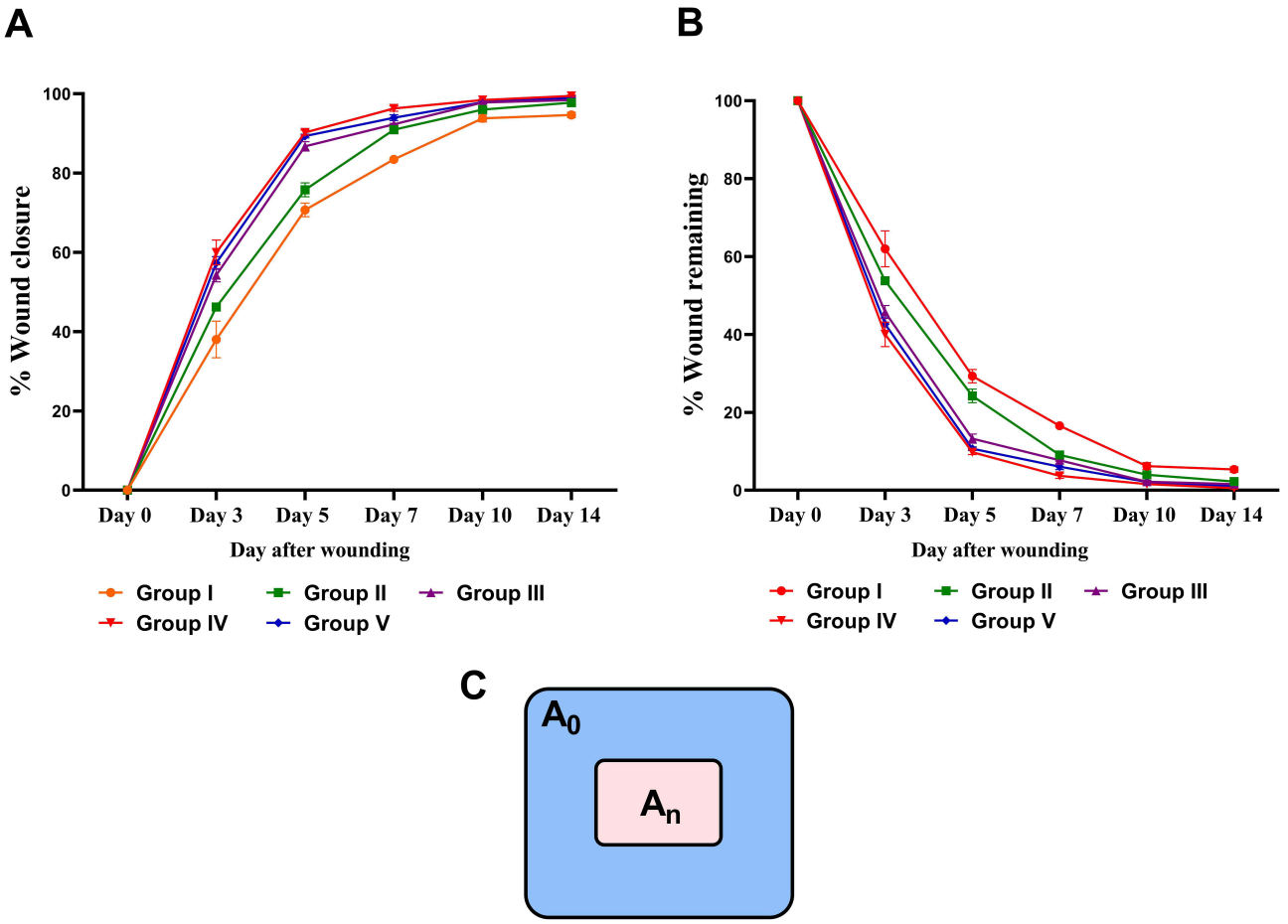

Figure 10 Quantitative analysis of wound healing; % wound closure (**A**), % wound remaining (**B**), and wound analysis (**C**).
Abbreviations: A_0, the original wound area on Day 0; A_n, the remaining wound area on indicated day.

94.65 ± 0.68, respectively, in the normal control group (Group I). In Group II, the % wound closure was insignificantly increased (46.19 ± 0.46, 75.78 ± 1.73, 90.93 ± 0.53, 96.01 ± 0.13 and 97.74 ± 0.51 on days 3, 5, 7, 10, and 14, respectively), indicating slower wound closure rates compared to Group I. On the other hand, the % wound closure was significantly enhanced in Group III, IV, and V when compared to Group I with the most significant increase noticed in Group IV followed by Group V. The % wound closure was 54.24 ± 1.67, 86.75 ± 1.18, 92.31 ± 0.20, 97.81 ± 0.37, and 98.42 ± 0.18 in Group III, 59.97 ± 3.12, 90.23 ± 0.63, 96.28 ± 0.68, 98.40 ± 0.22, and 99.47 ± 0.21 in Group IV, and 57.32 ± 1.58, 89.34 ± 0.47, 93.97 ± 0.73, 97.84 ± 0.39, and 99.00 ± 0.38 in Group V, at days 3, 5, 7, 10, and 14 days, respectively Figure 10A.

To sum up, Group IV had a significant increase in the wound closure rate developing a faster healing than other groups. Analogous findings would be found if the % wound remaining (Figure 10B) was used to compare the studied groups. F1 might act as a reservoir of CAR during the wound-healing process. CAR molecules might dissociate gradually from the phytosomal complex and diffuse out of the phospholipid matrix to reach the wound environment. At the same time, CAR was reported to act as a penetration enhancer.[110] Also, skin penetration might be further enhanced by the presence of phospholipid molecules that can disrupt the integrity of *SC* and fuse with it.[109] Hence, the effect of CAR-loaded phytosomes could boost re-epithelialization and epithelial cell differentiation at a faster rate than other treated groups. This would result in the formation of a thick epidermis during wound healing.[115]

Inflammation, re-epithelialization, and fibroblast cell proliferation were examined using H&E staining. Figure 11 shows microscopic pictures of the H&E-stained skin sections in the wound area. A delayed re-epithelialization with the presence of granulation tissue consisting of immature fibroblasts, few mononuclear cells, and many young capillary beds

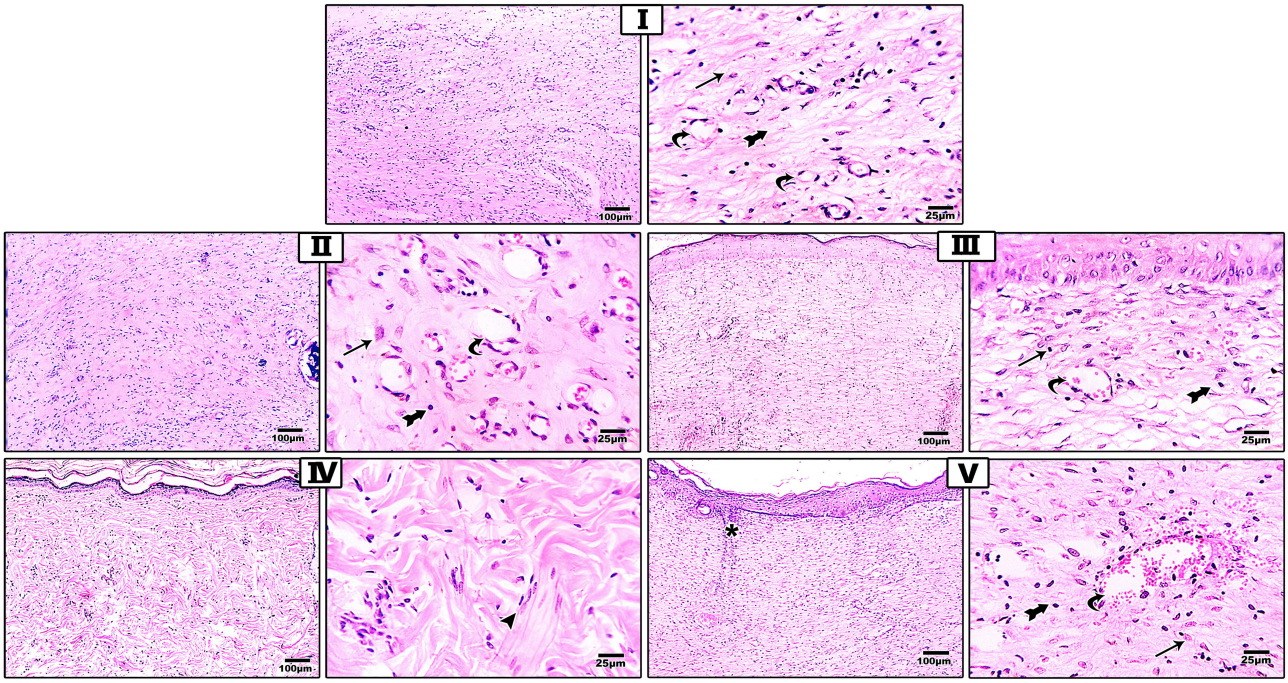

Figure 11 Histological evaluation of Groups I–V using H&E stain on the 14th day.
Notes: Black arrows point to immature fibroblasts, rocket arrows point to mononuclear cells, curved arrows point to young capillary beds, and arrowheads point to mature scar formation. H&E, 100× for bar 100 μm and 400× for bar 25 μm.
Abbreviation: H&E, hematoxylin and eosin staining.

filling wound gap could be observed in the normal control Group I, while Group II, III, and V displayed a complete re-epithelialization with the presence of granulation tissue consisting of immature fibroblasts, few mononuclear cells, many young capillary beds filling wound gap. On the other hand, the sections of Group IV showed entire re-epithelialization with mature scar formation filling the wound gap. From the previous findings, it is evident that the histological analysis of the rat skin was consistent with the findings of the macroscopic examination for wound healing evaluation.

Since collagen production is a necessary stage to guarantee full wound healing, Masson's trichrome stain (MT) was employed to estimate and analyze the intensity of collagen fiber deposition. Collagen was noticed as a blue-violet color. The stain was successfully used to indicate the collagen deposition as granulation tissue and matrix remodeling developed. The amount of total collagen fiber deposited was correlated with the blue stain's intensity.

Microscopic pictures of the MT-stained skin sections are shown in Figure 12. It was noted that there were disorganized thin bluish collagen strands filling the wound gap in normal control Group I. The skin sections of Group II demonstrated densely but still dis-organized bluish collagen strands filling the wound gap. Besides, Group III and V exhibited well-organized bluish collagen strands filling the wound gap. Finally, an accumulation of loosely arranged bluish mature collagen bundles at the wound site was observed in Group IV. These findings showed that the animals treated with F1-loaded hydrogel (Group IV) had the highest degree of collagen deposition among all treated groups, followed by the marketed cream group (Group V).

According to the histological examination, F1-loaded hydrogel could promote collagen deposition, which may be related to the anti-oxidative activity of CAR. The application of low molecular weight antioxidants like CAR is reported to consolidate collagen production and cellular proliferation at the site of the wound while lowering lipid peroxide levels.[116] Moreover, the Lipoid S100 might be incorporated into the structure of the cell membrane to reinforce the cellular proliferation of new fibroblasts with further accumulation of collagen. As a result, F1 could act as a lipid donor. Recently, several studies have shown extra roles of phospholipids during the wound healing phases. Lipids are suggested to act as intra- and inter-cellular mediators to modulate several cellular processes during tissue regeneration. They can mediate the attraction of immune cells and resolve anti-inflammatory responses.[117]

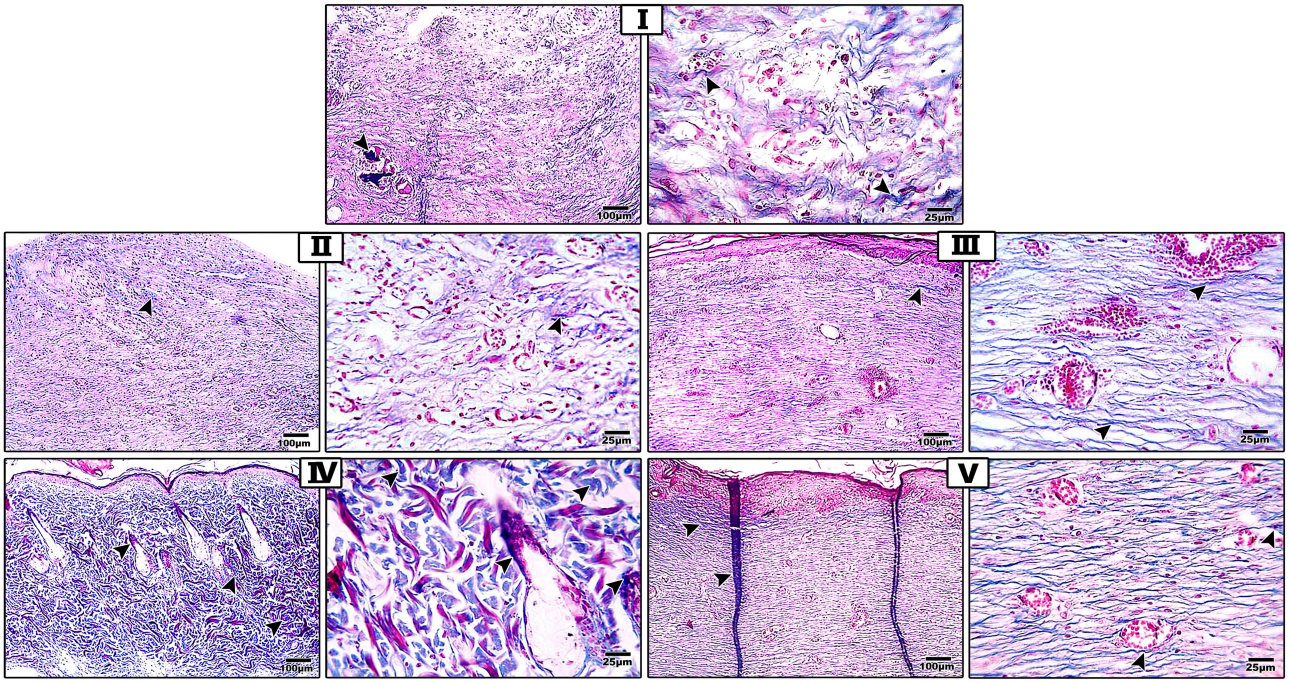

Figure 12 Histological evaluation of Groups I–V using MT stain on the 14th day.
Note: Arrowheads point to collagen strands. MT, 100× for bar 100 µm and 400× for bar 25 µm.
Abbreviation: MT, Masson's trichrome staining.

Anti-PCNA antibody immune-histochemical staining was used to evaluate the degree of epidermal cellular proliferation in the wound area. Microscopic pictures of the immune-stained skin sections against PCNA are present in Figure 13. A mild number of positive cells with brown nuclear staining were noticed in the normal control (Group I). Group II displayed increased numbers of positive cells with brown nuclear staining. Much increased numbers of positive cells with brown nuclear staining were found in Groups III and IV. For Group IV, more abundant positive cells with brown nuclear staining were observed.

These findings suggested that the CAR-loaded phytosomes could induce cell proliferation and support cellular regeneration by PCNA modulation. CAR has tissue remodeling and wound healing capacity.[118] Additionally, CAR was stated to act as a powerful inhibitor against pro-inflammatory damage in human keratinocytes.[119]

In the MT-stained sections, the percent deposition of collagen fibers was 6.012 ± 0.43%, 11.96 ± 0.63%, and 12.15 ± 0.58% in Groups I, II, and III, respectively. It was observed that the percent deposition of collagen fibers significantly increased in Groups II and III when compared to Group I ($p < 0.05$). The percent deposition of collagen fibers of Group IV and V were 24.65 ± 1.01% and 23.32 ± 0.89%, respectively ($p < 0.05$) (Figure 14A). Following the treatment with the F1-loaded hydrogel and the marketed cream, significantly more collagen fiber deposition was observed in Groups IV and V than in Group I ($p < 0.05$). Group IV exhibited the highest deposition level.

In the PCNA-stained sections, the mean area % of PCNA was 1.959 ± 0.37%, 2.427 ± 0.35%, and 2.558 ± 0.39% in Groups I, II, and III, respectively. The F1-loaded hydrogel and the marketed cream showed a significant increment of the mean area % of PCNA in Groups IV and V when compared to Groups I, II, and III ($p < 0.05$). The most significant increase was recognized in Group IV. The mean area % of PCNA of Groups IV and V were 6.654 ± 0.52% and 5.061 ± 0.36%, respectively ($p < 0.05$), as shown in Figure 14B.

Consequently, the macroscopic, histological examination and morphometric results confirmed that the better healing properties of F1-loaded hydrogel may be attributed to the ability of CAR to stimulate re-epithelialization, angiogenesis,

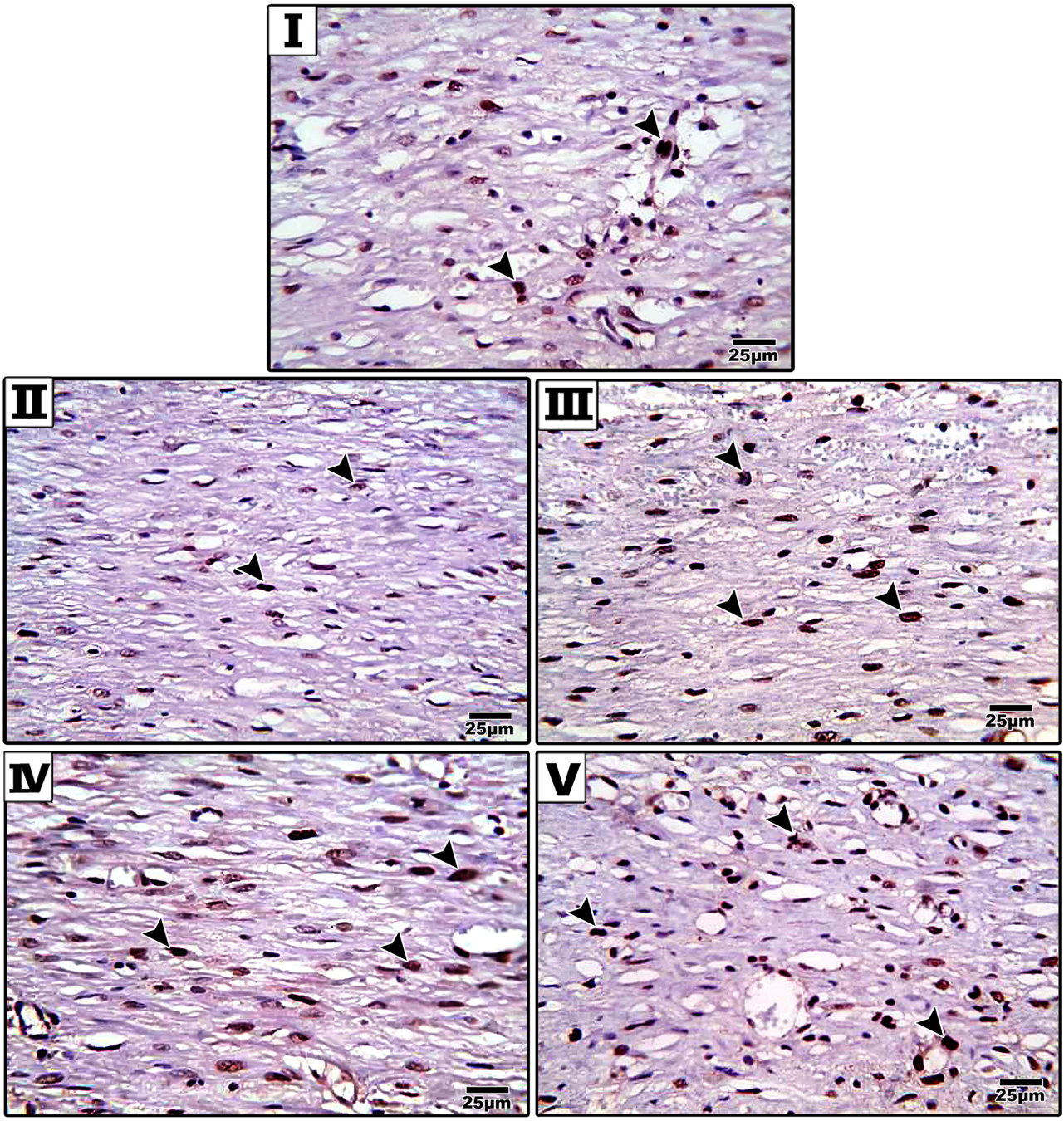

Figure 13 IHC evaluation of Groups I–V using PCNA antibody on the 14th day.
Note: Arrowheads point to positive cells. IHC counterstained with Mayer's hematoxylin, 400×.
Abbreviations: IHC, immunohistochemical; PCNA, proliferating cell nuclear antigen.

and collagen deposition. Besides, CAR has anti-inflammatory, antibacterial, and antioxidant properties.[12,13,15] These wound healing effects of CAR have been enhanced by incorporation into phytosomal complex. Thus, this phytosomal formula showed superior results over the marketed cream (Fucidin) and CAR alone.

Conclusion

In the present work, a topical NDDS of CAR-loaded phytosomal formulation has been developed to enhance its wound-healing properties. Initially, the molecular docking algorithm was found helpful in predicting the binding affinity between

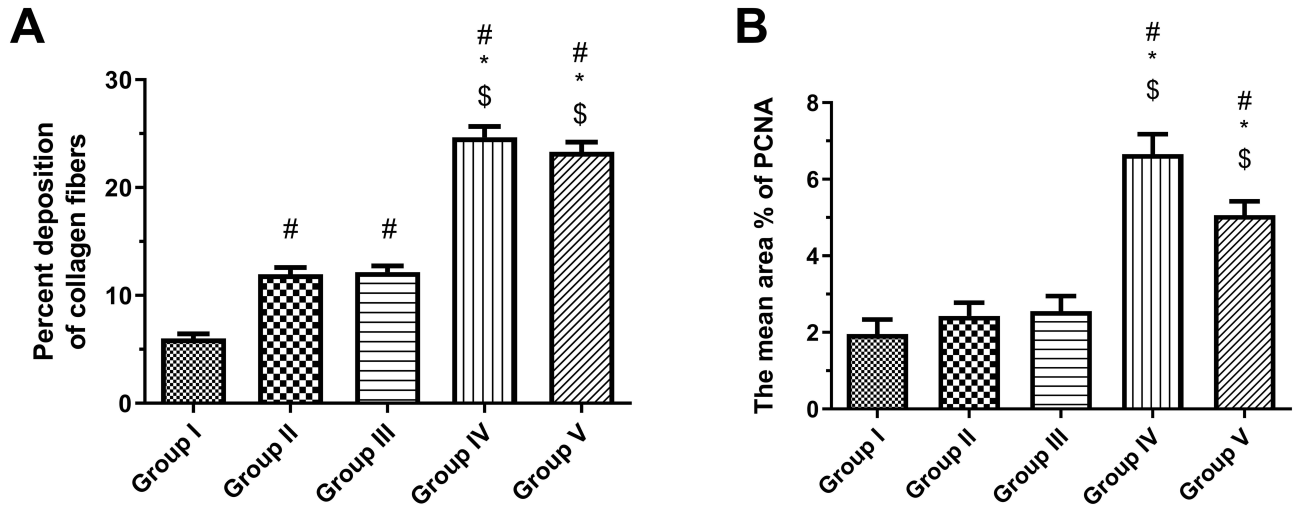

Figure 14 The percent deposition of collagen fibers (**A**) and the mean area % of PCNA (**B**) of Groups I–V on the 14th day.
Notes: Results are expressed as mean ± S.E., n = 6, $^{\#}P < 0.05$ compared with Group I, $^{*}P < 0.05$ compared with Group II, and $^{\$}P < 0.05$ compared with Group III.
Abbreviation: PCNA, proliferating cell nuclear antigen.

CAR and phospholipids. Then, CAR-loaded phytosomes were formulated, evaluated, and DoE-optimized. The optimal formula (F1) was characterized by enhancing the in vitro drug release and modulating the skin permeation over pure CAR. As well, the marked reduction of the wound area, more induction of collagen fiber deposition, and enhanced cellular proliferation of the F1-treated wounds confirmed that the wound-healing ability of CAR was significantly improved via its loading in F1. Considering the above outcomes, F1 could be considered as a potential wound-healing remedy, and hence, future studies could be planned to transfer our optimal formula to the clinical arena.

Data Sharing Statement

The datasets of the current study are available from the corresponding author upon a reasonable request.

Ethics Approval

The Research Ethical Committee at the Faculty of Pharmacy, Mansoura University approved protocols regarding animal experiments (Ethical Approval Code: 2023-39) in accordance with "The Principle of Laboratory Animal Care" (NIH publication No. 85-23, revised 1985). Also, the animal-related experiments were conducted in accordance with the Animal Research: Reporting of In Vivo Experiments (ARRIVE) principles.

Acknowledgments

Authors would like to express their appreciation to Lipoid GmbH (Ludwigshafen, Germany) for providing the phospholipids and to Mansoura University, Horus University, and AlMaarefa University for their help and support during the accomplishment of the present study.

Author Contributions

All authors made a significant contribution to the work reported, whether that is in the conception, study design, execution, acquisition of data, analysis and interpretation, or in all these areas; took part in drafting, revising or critically reviewing the article; gave final approval of the version to be published; have agreed on the journal to which the article has been submitted; and agree to be accountable for all aspects of the work.

Funding

The authors declare that no funds, grants, or other support were received during the preparation of this manuscript.

Disclosure

The authors declare no competing interests in this work.

References

1. Jones I, Currie L, Martin R. A guide to biological skin substitutes. *Br J Plast Surg*. 2002;55(3):185–193. doi:10.1054/bjps.2002.3800
2. Metcalfe AD, Ferguson MWJ. Bioengineering skin using mechanisms of regeneration and repair. *Biomaterials*. 2007;28(34):5100–5113. doi:10.1016/j.biomaterials.2007.07.031
3. Yildirimer L, Thanh NTK, Seifalian AM. Skin regeneration scaffolds: a multimodal bottom-up approach. *Trends Biotechnol*. 2012;30(12):638–648. doi:10.1016/j.tibtech.2012.08.004
4. Ibrahim N, Wong SK, Mohamed IN, et al. Wound healing properties of selected natural products. *Int J Environ Res Public Health*. 2018;15(11):2360. doi:10.3390/ijerph15112360
5. Thakur R, Jain N, Pathak R, Sandhu SS. Practices in wound healing studies of plants. *Evidence Based Complementary Alternative Med*. 2011;2011:438056. doi:10.1155/2011/438056
6. Harborne J. *Phytochemical Methods. A Guide to Modern Techniques of Plant Analysis*. 3 ed. Chapman & Hall, London: springer science & business media; 1973.
7. Chandel RS, Rastogi RP. Triterpenoid saponins and sapogenins: 1973–1978. *Phytochemistry*. 1980;19(9):1889–1908. doi:10.1016/0031-9422(80)83001-9
8. Tsala DE, Amadou D, Habtemariam S. Natural wound healing and bioactive natural products. *Phytopharmacology*. 2013;4(3):532–560.
9. Hosein Farzaei M, Abbasabadi Z, Reza Shams-Ardekani M, Abdollahi M, Rahimi R. A comprehensive review of plants and their active constituents with wound healing activity in traditional Iranian medicine. *Wounds*. 2014;26(7):197–206.
10. Gamit R, Nariya M, Acharya R, Shukla VJ. Wound healing potential of some medicinal plants with their screening models: a review. *Int J Med*. 2017;8(1):208–227.
11. Costa MF, Durço AO, Rabelo TK, Guimarães AG. Effects of Carvacrol, Thymol and essential oils containing such monoterpenes on wound healing: a systematic review. *J Pharm Pharmacol*. 2019;71(2):141–155. doi:10.1111/jphp.13054
12. Lima M, Quintans-Júnior LJ, de Santana WA, Martins Kaneto C, Pereira Soares MB, Villarreal CF. Anti-inflammatory effects of carvacrol: evidence for a key role of interleukin-10. *Eur J Pharmacol*. 2013;699(1):112–117. doi:10.1016/j.ejphar.2012.11.040
13. Marinelli L, Di Stefano A, Cacciatore I. Carvacrol and its derivatives as antibacterial agents. *Phytochemistry Reviews*. 2018;17(4):903–921. doi:10.1007/s11101-018-9569-x
14. Rúa J, Del Valle P, de Arriaga D, Fernández-álvarez L, García-Armesto MR. Combination of Carvacrol and Thymol: antimicrobial Activity Against Staphylococcus aureus and Antioxidant Activity. *Foodborne Pathog Dis*. 2019;16(9):622–629. doi:10.1089/fpd.2018.2594
15. André-Lévigne D, Modarressi A, Pepper MS, Pittet-Cuénod B. Reactive Oxygen Species and NOX Enzymes Are Emerging as Key Players in Cutaneous Wound Repair. *Int J Mol Sci*. 2017;18(10):2149. doi:10.3390/ijms18102149
16. Alvarez-Román R, Naik A, Kalia YN, Guy RH, Fessi H. Skin penetration and distribution of polymeric nanoparticles. *J Controlled Release*. 2004;99(1):53–62. doi:10.1016/j.jconrel.2004.06.015
17. Mordorski B, Prow T. Nanomaterials for wound healing. *Curr Dermatol Rep*. 2016;5(4):278–286. doi:10.1007/s13671-016-0159-0
18. Dantas AG, de Souza RL, de Almeida AR, et al. Development, Characterization, and Immunomodulatory Evaluation of Carvacrol-loaded Nanoemulsion. *Molecules*. 2021;26(13):3899. doi:10.3390/molecules26133899
19. Landry KS, Chang Y, McClements DJ, McLandsborough L. Effectiveness of a novel spontaneous carvacrol nanoemulsion against Salmonella enterica Enteritidis and Escherichia coli O157:H7 on contaminated mung bean and alfalfa seeds. *Int J Food Microbiol*. 2014;187:15–21. doi:10.1016/j.ijfoodmicro.2014.06.030
20. Galvão JG, Santos RL, Silva ARST, et al. Carvacrol loaded nanostructured lipid carriers as a promising parenteral formulation for leishmaniasis treatment. *Eur J Pharm Sci*. 2020;150:105335. doi:10.1016/j.ejps.2020.105335
21. He J, Huang S, Sun X, et al. Carvacrol Loaded Solid Lipid Nanoparticles of Propylene Glycol Monopalmitate and Glyceryl Monostearate: preparation, Characterization, and Synergistic Antimicrobial Activity. *Nanomaterials*. 2019;9(8):1162. doi:10.3390/nano9081162
22. Carvalho FO, Silva ÉR, Nunes PS, et al. Effects of the solid lipid nanoparticle of carvacrol on rodents with lung injury from smoke inhalation. *Naunyn-Schmiedeberg's Archives of Pharmacology*. 2020;393(3):445–455. doi:10.1007/s00210-019-01731-1
23. Engel JB, Heckler C, Tondo EC, Daroit DJ, da Silva Malheiros P. Antimicrobial activity of free and liposome-encapsulated thymol and carvacrol against Salmonella and Staphylococcus aureus adhered to stainless steel. *Int J Food Microbiol*. 2017;252:18–23. doi:10.1016/j.ijfoodmicro.2017.04.003
24. Tavares AG, Andrade J, Silva RRA, et al. Carvacrol-loaded liposome suspension: optimization, characterization and incorporation into poly (vinyl alcohol) films. *Food Funct*. 2021;12(14):6549–6557. doi:10.1039/D1FO00479D
25. Niza E, Božik M, Bravo I, et al. PEI-coated PLA nanoparticles to enhance the antimicrobial activity of carvacrol. *Food Chem*. 2020;328:127131. doi:10.1016/j.foodchem.2020.127131
26. Keawchaoon L, Yoksan R. Preparation, characterization and in vitro release study of carvacrol-loaded chitosan nanoparticles. *Colloids Surf B Biointerfaces*. 2011;84(1):163–171. doi:10.1016/j.colsurfb.2010.12.031
27. Chen F, Shi Z, Neoh KG, Kang ET. Antioxidant and antibacterial activities of eugenol and carvacrol-grafted chitosan nanoparticles. *Biotechnol Bioeng*. 2009;104(1):30–39. doi:10.1002/bit.22363
28. Maryam K, Shakeri S, Kiani K. Preparation and in vitro investigation of antigastric cancer activities of carvacrol-loaded human serum albumin nanoparticles. *IET Nanobiotechnol*. 2015;9(5):294–299. doi:10.1049/iet-nbt.2014.0040
29. Gholijani N, Abolmaali SS, Kalantar K, Ravanrooy MH. Therapeutic Effect of Carvacrol-loaded Albumin Nanoparticles on Arthritic Rats. *Iranian j Pharm Res*. 2020;19(1):312–320. doi:10.22037/ijpr.2019.15494.13131
30. Souza R, Dantas AGB, Melo C, Felício IM, Oliveira EE. Nanotechnology as a tool to improve the biological activity of carvacrol: a review. *J Drug Deliv Sci Technol*. 2022;76:103834. doi:10.1016/j.jddst.2022.103834

31. Barani M, Sangiovanni E, Angarano M, et al. Phytosomes as Innovative Delivery Systems for Phytochemicals: a Comprehensive Review of Literature. *Int J Nanomedicine*. 2021;16(2021):6983–7022. doi:10.2147/IJN.S318416
32. Bombardelli E, Patri GF. Complex compounds of bioflavonoids with phospholipids, their preparation and use, and pharmaceutical and cosmetic compositions containing them. *Google Patents*. 1991.
33. Kidd P, Head K. A review of the bioavailability and clinical efficacy of milk thistle phytosome: a silybin-phosphatidylcholine complex (Siliphos). *Altern Med Rev*. 2005;10(3):193–203.
34. Dewan N, Dasgupta D, Pandit S, Ahmed P. Review on-Herbosomes, A new arena for drug delivery. *J Pharm Phytochemistry*. 2016;5 (4):104–108.
35. Singh RP, Gangadharappa HV. Phospholipids: unique carriers for drug delivery systems. *J Drug Deliv Sci Technol*. 2017;39(2017):166–179. doi:10.1016/j.jddst.2017.03.027
36. Inc C. *Molecular operating environment (MOE)*. Chemical Computing Group Inc; 2016. 1010.
37. Elshal M, Eid N, El-Sayed I, El-Sayed W, Al-Karmalawy AA. Concanavalin-A Shows Synergistic Cytotoxicity with Tamoxifen viaInducing Apoptosis in Estrogen Receptor-Positive Breast Cancer: in vitro and Molecular Docking Studies. *Pharmaceutical Sci*. 2021;28(1):76–85.
38. Khattab M, Al-Karmalawy AA. Computational repurposing of benzimidazole anthelmintic drugs as potential colchicine binding site inhibitors. *Future Med Chem*. 2021;13(19):1623–1638. doi:10.4155/fmc-2020-0273
39. Parmar DR, Soni JY, Guduru R, et al. Discovery of new anticancer thiourea-azetidine hybrids: design, synthesis, in vitro antiproliferative, SAR, in silico molecular docking against VEGFR-2, ADMET, toxicity, and DFT studies. *Bioorg Chem*. 2021;115(2021):105206. doi:10.1016/j.bioorg.2021.105206
40. Al-Karmalawy AA, Farid MM, Mostafa A, et al. Naturally Available Flavonoid Aglycones as Potential Antiviral Drug Candidates against SARS-CoV-2. *Molecules*. 2021;26(21):6559. doi:10.3390/molecules26216559
41. Mahmoud DB, Bakr MM, Al-Karmalawy AA, Moatasim Y, El Taweel A, Mostafa A. Scrutinizing the feasibility of nonionic surfactants to form isotropic bicelles of curcumin: a potential antiviral candidate against COVID-19. *AAPS PharmSciTech*. 2022;23(1):1–12. doi:10.1208/s12249-021-02197-2
42. El-Far SW, Helmy MW, Khattab SN, Bekhit AA, Hussein AA, Elzoghby AO. Phytosomal bilayer-enveloped casein micelles for codelivery of Monascus yellow pigments and resveratrol to breast cancer. *Nanomedicine*. 2018;13(5):481–499. doi:10.2217/nnm-2017-0301
43. El-Menshawe SF, Ali AA, Rabeh MA, Khalil NM. Nanosized soy phytosome-based thermogel as topical anti-obesity formulation: an approach for acceptable level of evidence of an effective novel herbal weight loss product. *Int J Nanomedicine*. 2018;13(2018):307–318. doi:10.2147/IJN.S153429
44. Singh R, Parpani S, Narke R, Chavan R. Phytosome: recent advance research for novel drug delivery system. *Asian j Pharmaceutical Res Dev*. 2014;2(3):15–29.
45. Ahmed TA. Preparation of transfersomes encapsulating sildenafil aimed for transdermal drug delivery: plackett–Burman design and characterization. *J Liposome Res*. 2015;25(1):1–10. doi:10.3109/08982104.2014.950276
46. Jain A, Jain SK. In vitro release kinetics model fitting of liposomes: an insight. *Chem Phys Lipids*. 2016;201(2016):28–40. doi:10.1016/j.chemphyslip.2016.10.005
47. Hixson AW, Crowell JH. Dependence of Reaction Velocity upon surface and Agitation. *Ind Eng Chem*. 1931;23(8):923–931. doi:10.1021/ie50260a018
48. Weibull W. A Statistical Distribution Function of Wide Applicability. *J Appl Mechanics*. 2021;18(3):293–297. doi:10.1115/1.4010337
49. Langenbucher F. Letters to the Editor: linearization of dissolution rate curves by the Weibull distribution. *J Pharm Pharmacol*. 1972;24 (12):979–981. doi:10.1111/j.2042-7158.1972.tb08930.x
50. Higuchi T. Rate of Release of Medicaments from Ointment Bases Containing Drugs in Suspension. *J Pharm Sci*. 1961;50(10):874–875. doi:10.1002/jps.2600501018
51. Peppas NA. Analysis of Fickian and non-Fickian drug release from polymers. *Pharm Acta Helv*. 1985;60(4):110–111.
52. Costa P, Sousa Lobo JM. Modeling and comparison of dissolution profiles. *Eur J Pharm Sci*. 2001;13(2):123–133. doi:10.1016/S0928-0987(01)00095-1
53. Butani D, Yewale C, Misra A. Topical Amphotericin B solid lipid nanoparticles: design and development. *Colloids Surf B Biointerfaces*. 2016;139(2016):17–24. doi:10.1016/j.colsurfb.2015.07.032
54. Larrucea E, Arellano A, Santoyo S, Ygartua P. Interaction of Tenoxicam with Cyclodextrins and Its Influence on the In Vitro Percutaneous Penetration of the Drug. *Drug Dev Ind Pharm*. 2001;27(3):251–260. doi:10.1081/DDC-100000243
55. Ibrahim MMA, Sammour OA, Hammad MA, Megrab NA. In Vitro Evaluation of Proniosomes as a Drug Carrier for Flurbiprofen. *AAPS PharmSciTech*. 2008;9(3):782–790. doi:10.1208/s12249-008-9114-0
56. Kunta JR, Goskonda VR, Brotherton HO, Khan MA, Reddy IK. Effect of menthol and related terpenes on the percutaneous absorption of propranolol across excised hairless mouse skin. *J Pharm Sci*. 1997;86(12):1369–1373.
57. Jain P, Taleuzzaman M, Kala C, Kumar Gupta D, Ali A, Aslam M. Quality by design (Qbd) assisted development of phytosomal gel of aloe vera extract for topical delivery. *J Liposome Res*. 2021;31(4):381–388. doi:10.1080/08982104.2020.1849279
58. Mir M, Ahmed N, Permana AD, Rodgers AM, Donnelly RF, Rehman A. Enhancement in Site-Specific Delivery of Carvacrol against Methicillin Resistant Staphylococcus aureus Induced Skin Infections Using Enzyme Responsive Nanoparticles: a Proof of Concept Study. *Pharmaceutics*. 2019;11(11):606. doi:10.3390/pharmaceutics11110606
59. Bektas N, Şenel B, Yenilmez E, Özatik O, Arslan R. Evaluation of wound healing effect of chitosan-based gel formulation containing vitexin. *Saudi Pharm J*. 2020;28(1):87–94. doi:10.1016/j.jsps.2019.11.008
60. El-Aassar MR, Ibrahim OM, Fouda MMG, El-Beheri NG, Agwa MM. Wound healing of nanofiber comprising Polygalacturonic/Hyaluronic acid embedded silver nanoparticles: in-vitro and in-vivo studies. *Carbohydr Polym*. 2020;238(2020):116175. doi:10.1016/j.carbpol.2020.116175
61. Shamloo A, Aghababaie Z, Afjoul H, et al. Fabrication and evaluation of chitosan/gelatin/PVA hydrogel incorporating honey for wound healing applications: an in vitro, in vivo study. *Int J Pharm*. 2021;592(2021):120068. doi:10.1016/j.ijpharm.2020.120068
62. Jetten N, Roumans N, Gijbels MJ, et al. Wound administration of M2-polarized macrophages does not improve murine cutaneous healing responses. *PLoS One*. 2014;9(7):e102994. doi:10.1371/journal.pone.0102994

63. Murphy SV, Skardal A, Song L, et al. Solubilized amnion membrane hyaluronic acid hydrogel accelerates full-thickness wound healing. *Stem Cells Transl Med*. 2017;6(11):2020–2032. doi:10.1002/sctm.17-0053
64. Suvarna KS, Layton C, Bancroft JD. *Bancroft's theory and practice of histological techniques E-Book*. Elsevier Health Sciences; 2018.
65. Ebrahim N, Dessouky AA, Mostafa O, et al. Adipose mesenchymal stem cells combined with platelet-rich plasma accelerate diabetic wound healing by modulating the Notch pathway. *Stem Cell Res Ther*. 2021;12(1):392. doi:10.1186/s13287-021-02454-y
66. Lu M, Qiu Q, Luo X, et al. Phyto-phospholipid complexes (phytosomes): a novel strategy to improve the bioavailability of active constituents. *Asian J Pharm Sci*. 2019;14(3):265–274. doi:10.1016/j.ajps.2018.05.011
67. Anderson MJ, Whitcomb PJ. *RSM Simplified: Optimizing Processes Using Response Surface Methods for Design of Experiments*. 2nd ed. Productivity press; 2016.
68. Rasaee S, Ghanbarzadeh S, Mohammadi M, Hamishehkar H. Nano Phytosomes of Quercetin: a Promising Formulation for Fortification of Food Products with Antioxidants. *Pharmaceutical Sci*. 2014;20(3):96–101.
69. Verma DD, Verma S, Blume G, Fahr A. Particle size of liposomes influences dermal delivery of substances into skin. *Int J Pharm*. 2003;258 (1):141–151. doi:10.1016/S0378-5173(03)00183-2
70. Sinico C, Fadda AM. Vesicular carriers for dermal drug delivery. *Expert Opin Drug Deliv*. 2009;6(8):813–825. doi:10.1517/17425240903071029
71. Vikbjerg AF, Rusig J-Y, Jonsson G, Mu H, Xu X. Comparative Evaluation of the Emulsifying Properties of Phosphatidylcholine after Enzymatic Acyl Modification. *J Agric Food Chem*. 2006;54(9):3310–3316. doi:10.1021/jf052665w
72. Nii T, Ishii F. Dialkylphosphatidylcholine and egg yolk lecithin for emulsification of various triglycerides. *Colloids Surf B Biointerfaces*. 2005;41(4):305–311. doi:10.1016/j.colsurfb.2004.12.017
73. Surini S, Mubarak H, Ramadon D. Cosmetic Serum Containing Grape (Vitis vinifera L.) Seed Extract Phytosome: formulation and In Vitro Penetration Study. *J Young Pharmacists*. 2018;10(2s):S51–S55. doi:10.5530/jyp.2018.2s.10
74. Zhao L, Temelli F, Curtis JM, Chen L. Preparation of liposomes using supercritical carbon dioxide technology: effects of phospholipids and sterols. *Food Res Inte*. 2015;77(2015):63–72. doi:10.1016/j.foodres.2015.07.006
75. Danaei M, Dehghankhold M, Ataei S, et al. Impact of Particle Size and Polydispersity Index on the Clinical Applications of Lipidic Nanocarrier Systems. *Pharmaceutics*. 2018;10(2):57. doi:10.3390/pharmaceutics10020057
76. Ahmed MA, Al-mahallawi AM, El-Helaly SN, Abd-Elsalam WH. The effect of the saturation degree of phospholipid on the formation of a novel self-assembled nano-micellar complex carrier with enhanced intestinal permeability. *Int J Pharm*. 2019;569(2019):118567. doi:10.1016/j.ijpharm.2019.118567
77. Kaasalainen M, Mäkilä E, Riikonen J, et al. Effect of isotonic solutions and peptide adsorption on zeta potential of porous silicon nanoparticle drug delivery formulations. *Int J Pharm*. 2012;431(1):230–236. doi:10.1016/j.ijpharm.2012.04.059
78. Mohamed MI, Abdelbary AA, Kandil SM, Mahmoud TM. Preparation and evaluation of optimized zolmitriptan niosomal emulgel. *Drug Dev Ind Pharm*. 2019;45(7):1157–1167. doi:10.1080/03639045.2019.1601737
79. Maryana W, Rachmawati H, Mudhakir D. Formation of Phytosome Containing Silymarin Using Thin Layer-Hydration Technique Aimed for Oral Delivery. *Materials Today*. 2016;3(3):855–866.
80. Zhu S, Luo C, Feng W, et al. Selenium-deposited tripterine phytosomes ameliorate the antiarthritic efficacy of the phytomedicine via a synergistic sensitization. *Int J Pharm*. 2020;578(2020):119104. doi:10.1016/j.ijpharm.2020.119104
81. Siddiqui L, Bag J, Seetha S, et al. Assessing the potential of lignin nanoparticles as drug carrier: synthesis, cytotoxicity and genotoxicity studies. *Int J Biol Macromol*. 2020;152(2020):786–802. doi:10.1016/j.ijbiomac.2020.02.311
82. Pawar HA, Bhangale BD. Phytosome as a novel biomedicine: a microencapsulated drug delivery system. *J Bioanal Biomed*. 2015;7(1):6–12.
83. Hth V, Hook SM, Siqueira SD, Müllertz A, Rades T, McDowell A. Are phytosomes a superior nanodelivery system for the antioxidant rutin? *Int J Pharm*. 2018;548(1):82–91. doi:10.1016/j.ijpharm.2018.06.042
84. Sun C, Cao J, Wang Y, et al. Preparation and characterization of pectin-based edible coating agent encapsulating carvacrol/HPβCD inclusion complex for inhibiting fungi. *Food Hydrocoll*. 2022;125(2022):107374. doi:10.1016/j.foodhyd.2021.107374
85. Ittadwar PA, Puranik PK. Novel umbelliferone phytosomes: development and optimization using experimental design approach and evaluation of photo-protective and antioxidant activity. *Int J Pharm Pharmaceutical Sci*. 2017;9(1):218–228. doi:10.22159/ijpps.2017v9i1.14635
86. Chi C, Zhang C, Liu Y, Nie H, Zhou J, Ding Y. Phytosome-nanosuspensions for silybin-phospholipid complex with increased bioavailability and hepatoprotection efficacy. *Eur J Pharm Sci*. 2020;144(2020):105212. doi:10.1016/j.ejps.2020.105212
87. Tavares AG, Andrade J, Silva RRA, et al. Carvacrol-loaded liposome suspension: optimization, characterization and incorporation into poly (vinyl alcohol) films. *Food Funct*. 2021;12(14):6549–6557.
88. Das MK, Kalita B. Design and evaluation of phyto-phospholipid complexes (phytosomes) of rutin for transdermal application. *J Applied Pharm Sci*. 2014;4(10):051–057. doi:10.7324/JAPS.2014.401010
89. Pereira A, Mallya R. Formulation and evaluation of a photoprotectant cream containing Phyllanthus emblica extract-phospholipid complex. *J Pharm Phytochemistry*. 2015;4(2):232–240.
90. Freag MS, Elnaggar YS, Abdallah OY. Lyophilized phytosomal nanocarriers as platforms for enhanced diosmin delivery: optimization and ex vivo permeation. *Int J Nanomedicine*. 2013;8(2013):2385. doi:10.2147/IJN.S45231
91. Taghizadeh Z, Rakhshani S, Jahani V, Rajabi O, Haghighi HM, Abbaspour M. Preparation and in vitro characterization of carvacrol pellets by combination of liquisolid technique and extrusion-spheronization. *J Drug Deliv Sci Technol*. 2021;61(2021):102232. doi:10.1016/j.jddst.2020.102232
92. Gupta NK, Dixit VK. Bioavailability Enhancement of Curcumin by Complexation with Phosphatidyl Choline. *J Pharm Sci*. 2011;100 (5):1987–1995. doi:10.1002/jps.22393
93. Maiti K, Mukherjee K, Gantait A, Saha BP, Mukherjee PK. Curcumin–phospholipid complex: preparation, therapeutic evaluation and pharmacokinetic study in rats. *Int J Pharm*. 2007;330(1):155–163. doi:10.1016/j.ijpharm.2006.09.025
94. Ebada HMK, Nasra MMA, Elnaggar YSR, Abdallah OY. Novel Rhein–phospholipid complex targeting skin diseases: development, in vitro, ex vivo, and in vivo studies. *Drug Deliv Transl Res*. 2021;11(3):1107–1118. doi:10.1007/s13346-020-00833-1
95. Freag MS, Saleh WM, Abdallah OY. Self-assembled phospholipid-based phytosomal nanocarriers as promising platforms for improving oral bioavailability of the anticancer celastrol. *Int J Pharm*. 2018;535(1):18–26. doi:10.1016/j.ijpharm.2017.10.053

96. Zhang J, Peng Q, Shi S, et al. Preparation, characterization, and in vivo evaluation of a self-nanoemulsifying drug delivery system (SNEDDS) loaded with morin-phospholipid complex. *Int J Nanomedicine*. 2011;6(2011):3405–3414. doi:10.2147/IJN.S25824
97. Hou Z, Li Y, Huang Y, et al. Phytosomes Loaded with Mitomycin C–Soybean Phosphatidylcholine Complex Developed for Drug Delivery. *Mol Pharm*. 2013;10(1):90–101. doi:10.1021/mp300489p
98. Alhakamy NA, Badr-Eldin SM, Fahmy A, et al. Thymoquinone-Loaded Soy-Phospholipid-Based Phytosomes Exhibit Anticancer Potential against Human Lung Cancer Cells. *Pharmaceutics*. 2020;12(8):761. doi:10.3390/pharmaceutics12080761
99. Cedillo-Flores OE, Rodríguez-Laguna N, Hipólito-Nájera AR, Nivón-Ramírez D, Gómez-Balderas R, Moya-Hernández R. Effect of the pH on the thermodynamic stability of inclusion complexes of thymol and carvacrol in β-cyclodextrin in water. *Food Hydrocoll*. 2022;124 (2022):107307. doi:10.1016/j.foodhyd.2021.107307
100. Perrut M, Jung J, Leboeuf F. Enhancement of dissolution rate of poorly-soluble active ingredients by supercritical fluid processes: part I: micronization of neat particles. *Int J Pharm*. 2005;288(1):3–10. doi:10.1016/j.ijpharm.2004.09.007
101. Dash S, Murthy PN, Nath L, Chowdhury PJAPP. Kinetic modeling on drug release from controlled drug delivery systems. *Acta Poloniae Pharmaceutica*. 2010;67(3):217–223.
102. Telange DR, Patil AT, Pethe AM, Fegade H, Anand S, Dave VS. Formulation and characterization of an apigenin-phospholipid phytosome (APLC) for improved solubility, in vivo bioavailability, and antioxidant potential. *Eur J Pharm Sci*. 2017;108(2017):36–49. doi:10.1016/j.ejps.2016.12.009
103. Papadopoulou V, Kosmidis K, Vlachou M, Macheras P. On the use of the Weibull function for the discernment of drug release mechanisms. *Int J Pharm*. 2006;309(1):44–50. doi:10.1016/j.ijpharm.2005.10.044
104. Ignacio M, Chubynsky MV, Slater GW. Interpreting the Weibull fitting parameters for diffusion-controlled release data. *Physica A*. 2017;486 (2017):486–496. doi:10.1016/j.physa.2017.05.033
105. Martínez L, Villalobos R, Sánchez M, Cruz J, Ganem A, Melgoza LM. Monte Carlo simulations for the study of drug release from cylindrical matrix systems with an inert nucleus. *Int J Pharm*. 2009;369(1):38–46. doi:10.1016/j.ijpharm.2008.10.023
106. Păvăloiu R-D, Sha'at F, Bubueanu C, et al. Polyphenolic Extract from Sambucus ebulus L. Leaves Free and Loaded into Lipid Vesicles. *Nanomaterials*. 2020;10(1):56. doi:10.3390/nano10010056
107. Siepmann J, Peppas NA. Modeling of drug release from delivery systems based on hydroxypropyl methylcellulose (HPMC). *Adv Drug Deliv Rev*. 2012;64(2012):163–174. doi:10.1016/j.addr.2012.09.028
108. Kirjavainen M, Urtti A, Jääskeläinen I, et al. Interaction of liposomes with human skin in vitro — the influence of lipid composition and structure. *Biochimica et Biophysica Acta*. 1996;1304(3):179–189. doi:10.1016/S0005-2760(96)00126-9
109. Spernath A, Aserin A, Sintov AC, Garti N. Phosphatidylcholine embedded micellar systems: enhanced permeability through rat skin. *J Colloid Interface Sci*. 2008;318(2):421–429. doi:10.1016/j.jcis.2007.10.036
110. Suntres ZE, Coccimiglio J, Alipour M. The Bioactivity and Toxicological Actions of Carvacrol. *Crit Rev Food Sci Nutr*. 2015;55(3):304–318. doi:10.1080/10408398.2011.653458
111. Grip J, Engstad RE, Skjæveland I, Škalko-Basnet N, Holsæter AM. Sprayable Carbopol hydrogel with soluble beta-1,3/1,6-glucan as an active ingredient for wound healing – development and in-vivo evaluation. *Eur J Pharm Sci*. 2017;107(2017):24–31. doi:10.1016/j.ejps.2017.06.029
112. Garg T, Rath G, Goyal AK. Comprehensive review on additives of topical dosage forms for drug delivery. *Drug Deliv*. 2015;22(8):969–987. doi:10.3109/10717544.2013.879355
113. Tenci M, Rossi S, Aguzzi C, et al. Carvacrol/clay hybrids loaded into in situ gelling films. *Int J Pharm*. 2017;531(2):676–688. doi:10.1016/j.ijpharm.2017.06.024
114. Mir M, Permana AD, Ahmed N, Khan GM, Rehman A, Donnelly RF. Enhancement in site-specific delivery of carvacrol for potential treatment of infected wounds using infection responsive nanoparticles loaded into dissolving microneedles: a proof of concept study. *Eur J Pharmaceutics Biopharmaceutics*. 2020;147:57–68. doi:10.1016/j.ejpb.2019.12.008
115. Takzaree N, Hadjiakhondi A, Hassanzadeh G, Rouini MR, Manayi A, Zolbin MM. Transforming growth factor-β (TGF-β) activation in cutaneous wounds after topical application of aloe vera gel. *Can J Physiol Pharmacol*. 2016;94(12):1285–1290. doi:10.1139/cjpp-2015-0460
116. Nasab ME, Takzaree N, Saffari PM, Partoazar A. In vitro antioxidant activity and in vivo wound-healing effect of lecithin liposomes: a comparative study. *J Comp Eff Res*. 2019;8(8):633–643. doi:10.2217/cer-2018-0128
117. Pils V, Terlecki-Zaniewicz L, Schosserer M, Grillari J, Lämmermann I. The role of lipid-based signalling in wound healing and senescence. *Mech Ageing Dev*. 2021;198(2021):111527. doi:10.1016/j.mad.2021.111527
118. Licata M, Tuttolomondo T, Dugo G, et al. Study of quantitative and qualitative variations in essential oils of Sicilian oregano biotypes. *J Essential Oil Res*. 2015;27(4):293–306. doi:10.1080/10412905.2015.1045088
119. Avola R, Granata G, Geraci C, Napoli E, Graziano ACE, Cardile V. Oregano (Origanum vulgare L.) essential oil provides anti-inflammatory activity and facilitates wound healing in a human keratinocytes cell model. *Food Chem Toxicol*. 2020;144(2020):111586. doi:10.1016/j.fct.2020.111586